

0020 0014

CHG  
Item 29

Fluid Inclusions and Hydrothermal Alteration  
on the Dixie Valley Fault, Nevada

by

W. T. Parry, D. Hedderly-Smith, and R. L. Bruhn

Department of Geology and Geophysics

University of Utah

Salt Lake City, Utah 84112-1183

**Abstract**

Footwall rocks of the 1954 rupture segment of the Dixie Valley fault show extensive hydrothermal alteration related to fluids that were present on the fault during tectonic events. Hydrothermal alteration of granitic host rocks consists of temporally and spatially overlapping mineral assemblages. An early, biotite-feldspar assemblage is followed by later Fe-chlorite and epidote. Both chlorite and epidote are replaced by hydrothermal sericite and cut by calcite-hematite veins. Local areas of prehnite are present. The latest hydrothermal minerals are stilbite, laumontite, kaolinite, alunite, smectite, and illite. Coarse quartz-calcite veins, pervasive replacement of rock units with fine grained quartz, and later replacement of volcanic and plutonic rocks with chalcedony and opal accompanied the alteration.

Secondary fluid inclusions trapped in healed microfractures in igneous quartz include (1) liquid rich, moderate salinity inclusions, (2) inclusions that contain a moderate salinity aqueous liquid and  $\text{CO}_2$ , (3) inclusions that show eutectic melting temperatures below the  $\text{NaCl-H}_2\text{O}$  eutectic and contain substantial  $\text{CaCl}_2$ , and (4) inclusions containing halite and other daughter minerals. Microthermometric measurements on these inclusions yield variable compositions and homogenization temperatures. Salinities of liquid rich, moderate salinity inclusions varies from 0.1 to 12.9 weight percent  $\text{NaCl}$  with

the mode in the interval 0 to 1%. Salinities of CO<sub>2</sub> bearing inclusions ranges from 0.62 to 6.81 weight % NaCl relative to H<sub>2</sub>O, and salinities of inclusions with low eutectic melting temperatures are 12.9 to 25.3 weight % NaCl equivalent. Salinities of halite bearing inclusions are 30.1 to 39.2 weight % NaCl. Homogenization temperatures span the range 120° to 400° C, with higher temperature inclusions in the southern sericite alteration zone.

Variable fluid inclusion compositions, homogenization temperatures and densities represent several different fluids that have been subjected to the processes of isochemical cooling with upward displacement of the footwall, mixing of cool low-salinity water with hotter components, and mixing of cool, evaporite brine with hotter components.

The P-T path of the fault fluids is established by mineral equilibria and fluid inclusion characteristics. The path includes a lithostatic fluid pressure at 305°C and 1570 bars. Along with cooling and escape of CO<sub>2</sub> from fluids, the fluid P-T path probably approaches hydrostatic pressure conditions at lower temperatures.

Hydrothermal alteration product minerals, fluid temperatures, pressures, and compositions in the footwall of the Dixie Valley fault constrain minimum fault age to 20 to 25 Ma, displacement to 6 km with about 3 km of pre 10 to 13 Ma and 3 km of post 10 Ma uplift. Fluid compositions and P-T data suggest the following mechanism for rupture initiation and arrest. Ruptures may be initiated as a result of high fluid pressures, then opening of dilatant fractures causes drastic decrease in fluid pressure, separation of steam and CO<sub>2</sub>. The drastic reduction in fluid bulk modulus that accompanies volatile separation permits propagation of the ruptures even though fluid pressure is reduced. In areas where fluid pressure reduction is not accompanied by phase

separation, fractures are arrested by dilatant hardening.

### Introduction

Hydrothermal fluids play a significant role in the mechanical stability of faults. Increased fluid pressure reduces the frictional shear strength of an existing fault where failure is governed by effective stress (Hubbert and Rubey, 1959). Alteration of the fault rock to mineral assemblages such as muscovite with lower frictional or flow strength decrease stability (Janecke and Evans, 1988; Kirby and Kronenberg, 1987). Increased pore volume produced during dynamic rupturing with accompanying reduction in fluid pressure (Ismail and Murrell, 1976; Rudnicki and Chen, 1988; Roeloffs and Rudnicki, 1985), and healing and sealing of cracks with precipitated minerals increase stability. Fault stability is also related to the physical state of the fault zone and the constitutive properties of fault zone rock and fluids. New pore volume produced by dilatancy coupled with low rock permeability can result in decompression of the fluid and may stabilize rupture. Separation of the fluid into gas and liquid phases results in drastic reduction in fluid bulk modulus that diminishes the dilatant hardening effect and may permit rupture propagation (Rudnicki and Chen, 1988; Parry and Bruhn, 1990).

Evidence of hydrothermal fluid circulation and chemical interaction of fluids with fault zone rocks is evident in fault zones exhumed by erosion (Sibson, 1981; Sibson, et al., 1988; Parry et al., 1988). Microscopic to megascopic fractures filled with precipitated minerals are common, and fluid inclusions trapped within these minerals represent samples of the pore fluids. Characteristics of fluid inclusions together with associated hydrothermal alteration product minerals may be used to infer the physical state of the fault zone at depth, estimate constitutive properties of fault zone materials

such as fluid bulk modulus which control fault stability (Parry and Bruhn, 1990), constrain the fluid pressure (Parry and Bruhn, 1986 ; Parry et al., 1988; Parry and Bruhn, 1990) and estimate fault displacement using pressure and temperature constraints (Parry and Bruhn, 1987).

The Dixie Valley fault system is part of a 300 km long active seismic belt in central Nevada (Wallace, 1984) with individual segments capable of producing magnitude 7 earthquakes. Exhumed footwall rocks on segments of this fault display the effects of hydrothermal alteration and provide an opportunity for observation of fluid characteristics in fluid inclusions and alteration product mineralogy near seismogenic depths on the fault.

The objectives of this study are to characterize and map hydrothermal alteration assemblages on the footwall of the 1954 rupture segment of the Dixie Valley fault Nevada, determine the characteristics of fault pore fluids using fluid inclusions and alteration mineralogy, and to relate these characteristics to fault behavior and history. We have chosen the 1954 rupture segment for study because the footwall exposes Tertiary age granitic rocks in which aluminosilicate minerals provide an excellent record of chemical interaction of fluids, and the age of the alteration must postdate the emplacement of the igneous host rock.

#### **The Dixie Valley Fault**

The Dixie Valley fault in the western Basin and Range province of Nevada lies in an area of high heat flow, recent, voluminous volcanic activity, and recent seismic activity. Historic seismicity has resulted in surface rupturing events (from north to south) at Pleasant Valley (1915), Fairview Peak-Dixie Valley (1954), Wonder (1903), Cedar Mountains (1932), Excelsior Mountain (1934), Mammoth Lakes (1980), and Owens Valley (1972) (Wallace and

Whitney, 1984).

The Dixie Valley fault system forms the eastern margin of the Stillwater Mountains shown in Figure 1, and close spatial correlation between the 1954 and older fault scarps indicates that repeated surface-rupturing earthquakes have created the structural relief between the Stillwater mountains and Dixie Valley. Footwall rocks exposed in the Stillwater range shown in Figure 2 include Mesozoic sedimentary rocks intruded by the Jurassic gabbroic Humboldt lopolith (Willden and Speed, 1974), a multiphase Oligocene granodiorite-quartz monzonite-granite intrusion emplaced at 28 Ma (Speed and Armstrong, 1971), and a small Cretaceous granitic intrusion. These rocks are overlain by Tertiary volcanic rocks.

Dixie Valley is a graben system consisting of an inner graben with valley fill 2 to 3.2 km deep and a shallower outer graben containing 150 to 1,500 m of fill (Meister, 1967; Thompson and Burke, 1973; Okaya and Thompson, 1985; Anderson, et al., 1983). Fault displacement has taken place along a normal fault at the base of the Stillwater range (the range front fault) and along a zone of faults a few km east of the range front (the piedmont fault zone) (Bell and Katzer, 1987, 1990).

The topographic low in Dixie Valley is dominated by a large playa and the Humboldt salt marsh occupies 46 square miles of Dixie Valley at an elevation of 3365' (Bateman and Hess, 1978). The brine is 28.7 to 38.7 weight percent salt.

#### Experimental Procedures

Our studies focus on hydrothermal alteration and fluid inclusion characteristics in footwall granitic and volcanic rocks of the 1954 rupture segment of the Dixie Valley fault. Samples were collected from outcrop of the

intrusive and volcanic rocks in the footwall of the Dixie Valley fault at localities shown in Figure 3. Hydrothermal alteration mineral assemblages, tectonic textures, and fluid inclusions were studied in 183 thin sections of rocks collected during the course of mapping footwall alteration. Alteration mineralogy and tectonic textures were determined by a combination of petrographic microscope and x-ray diffraction techniques. Clay minerals were identified by X-ray diffraction of oriented smears of clay size material following vapor glycolation at 60°C and heating to 250° and 550°C. The relative ages of alteration assemblages is established from cross-cutting and replacement relationships.

Identity, density, and homogenization temperatures of fluid-inclusion contents were determined by observation of phase changes in doubly polished plates on a Fluid Inc. heating-freezing microscope stage and procedures outlined by Roedder (1984), Parry and Bruhn (1986), Parry (1986), and Parry et al. (1988). Temperature calibration for the microscope stage was accomplished using synthetic fluid inclusions of known composition (Sterner and Bodnar, 1984). Phase changes that were used to characterized fluid inclusion fluids were the CO<sub>2</sub> triple point temperature, melting of clathrate (Collins, 1979; Bozzo et al., 1975), melting of ice, hydrohalite, and halite, CO<sub>2</sub> liquid-vapor homogenization, and overall homogenization of fluid inclusion contents.

Fluid inclusion salinities were estimated from ice melting temperatures, from clathrate melting temperatures, and from halite melting temperatures as appropriate. Salinities of fluids in inclusions with no detectable CO<sub>2</sub> were calculated using freezing point depression estimated from ice melting temperatures and the regression equation of Potter et al. (1978). Salinities

for fluid inclusions on the halite liquidus were calculated using the equation and coefficients of Sterner et. al (1988). Salinity of fluid inclusions showing eutectic temperatures below the NaCl-H<sub>2</sub>O eutectic were estimated using the equations and coefficients for total salinity of Oakes et al. (1990). Salinity of fluid inclusion fluids containing a halite daughter salt were estimated using the techniques and data of Vanko, et al.(1988).

The greatest source of error in fluid inclusion measurements is a consequence of post entrapment changes in secondary inclusions described as necked inclusions by Roedder (1984) and termed maturation by Bodnar et al. (1985). These changes result from dissolution and reprecipitation of host mineral surrounding the trapped fluid. The initial fluid inclusion may be irregularly shaped but in time necks down to form many smaller inclusions with more regular shapes and often varying liquid to vapor ratios. We have avoided measurements of necked inclusions. Fluid inclusions in close proximity to one another with widely varying liquid to vapor ratios were not measured, and inclusions near one another with apparently similar liquid-vapor ratios were checked to insure similar homogenization temperatures.

#### **Fault Rock Petrography and Alteration**

Four intrusive plutons in the intrusive complex shown in Figures 2 and 3 were recognized in the footwall of the 1954 rupture segment during our field investigations, but the contacts between separate plutons were not mapped. They are, from south to north, granite (40% plagioclase, 33% K-feldspar, 25% quartz, 2% biotite) outcropping in the vicinity of A in Figure 2; granodiorite (62% plagioclase, 12% K-feldspar, 19% quartz, 7% biotite) outcropping in the vicinity of B in Figure 2; biotite quartz monzonite (26 % plagioclase, 34% K-feldspar, 27 % biotite, 8% hornblende, 9% quartz) outcropping in the vicinity

of C in Figure 2; and a small granite to granodiorite stock near Alameda Canyon (D on Figure 2) that consists of 33 % quartz, 43% plagioclase, 17% K-feldspar, and 7% biotite. The K-Ar age of biotite from the biotite quartz monzonite at locality #108, Figure 3, is  $28 \pm 2$  Ma (Table 1) (Speed and Armstrong, 1971). The granite is younger than the granodiorite, but the relative age of the granodiorite with respect to the biotite quartz monzonite is not known due to the lack of outcrop. The K-Ar age of muscovite from the Alameda Canyon pluton at D on Figure 2 is  $78.4 \pm 2.9$  Ma (Table 1). Additional smaller intrusive rocks are also present at map localities shown in Figure 3 and include an altered quartz latite porphyry dike at #37, a diorite dike at #17, a quartz diorite dike at #65 and a diorite dike at #97. These smaller bodies are too small to map at the scale of Figures 2 and 3.

Fault breccia and cataclasite directly overlie the footwall granitic rocks. A pervasive set of closely spaced extension fractures is concentrated in the footwall immediately adjacent to the fault. Spacing between these steeply east-dipping extension fractures is only a few centimeters and these fractures are present throughout the breccia and within the footwall for several meters to 10's of meters. Thin discontinuous shear planes subparallel to the main fault plane also extend into the footwall and coexist with the penetrative fracture set.

Cataclasite is the dominant fault rock. Cataclastic textures include pervasive fracturing of large volumes of rock and veins. Cataclastic veins are thin tabular and branching bodies of fine cataclasite consisting of angular fragments of quartz and feldspar occasionally with a matrix of sericite or chlorite. No shear displacement of the fracture walls is apparent in thin section even though the fractures are crowded with angular

fragments of quartz and feldspar and the quartz may be stretched, show undulatory extinction and recrystallization. We infer that the cataclasite was emplaced as a suspension of fine rock particles possibly during hydraulic fracturing.

Temporally and spatially overlapping hydrothermal alteration mineral assemblages occur as a narrow band near the 1954 rupture in the fault footwall. Geometric association of the alteration with the fault and association with tectonic textures indicate alteration mineral assemblages are related to tectonic events on the Dixie Valley fault. From earliest to latest, these assemblages are biotite+K-feldspar, chlorite+epidote, sericite+kaolinite+smectite, prehnite+laumontite+stilbite+kaolinite+smectite. The spatial distribution of areas dominated by sericite, chlorite+epidote, and zeolite assemblages is shown in Figure 3. The sericitic alteration is superimposed on chlorite and epidote, traces of which remain in the rock. Prehnite, laumontite, stilbite, and clay minerals have also been superimposed on earlier alteration mineralogies with traces of the earlier minerals remaining in the rock.

The earliest assemblage of hydrothermal minerals includes a pervasive, partial to complete replacement of igneous plagioclase by K-feldspar, leaving patchy remnants of twinned plagioclase cross-cut by K-feldspar veins. Hydrothermal K-feldspar also occurs as selvages on quartz veins and as quartz+K-feldspar veins. Later veins of albite also crosscut plagioclase. Hydrothermal K-feldspar was not mapped but is widely distributed along the fault footwall. Hydrothermal biotite also forms early in the sequence, though the relative age of biotite cannot be unequivocally tied to the K-feldspar replacement of plagioclase. Hydrothermal biotite occurs as thin

veins, as replacement of hornblende and as a replacement of igneous biotite. Hydrothermal biotite is more abundant in more mafic rocks where biotite vein networks occur in plagioclase and pyroxene. Hydrothermal biotite is not volumetrically abundant anywhere in the fault footwall.

The dominant alteration mineralogy on the Dixie Valley fault footwall is Fe-chlorite and epidote associated with local areas of calcite, hematite, sericite, and prehnite. Chlorite replaces hornblende and biotite and occurs in veins with actinolite, green biotite, calcite, quartz, or epidote. Epidote forms a selvage to quartz+epidote veins that reach thicknesses of several centimeters. Cataclasite and breccia consisting of epidote and chlorite form the faces of some of the faceted spurs.

Hydrothermal sericite (dioctahedral white mica) replaces all previously formed minerals except quartz. In the most intense sericitic alteration, feldspars have been nearly completely replaced by sericite and fine-grained quartz forming an altered rock with up to 58% sericite with the remainder of the rock relict igneous quartz and fine grained hydrothermal quartz. Biotite, hornblende, chlorite and epidote are completely replaced by sericite. With decreasing intensity of alteration sericite occurs as disseminated grains within the feldspars and as isolated veins. X-ray diffraction of clay size separates from sericitized rocks shows both kaolinite and smectite associated with the sericite. However thin section examination shows the kaolinite and smectite are later than the sericite.

Prehnite occurs locally as fibrous, radiating masses with typical bow-tie extinction partially replacing biotite.

Latest hydrothermal minerals are laumontite, stilbite, kaolinite, smectite, and very fine grained illite that occur on the fronts of faceted

spurs. Silicification of both volcanic and plutonic rocks is the latest alteration event. Chalcedony, kaolinite, alunite, smectite, and opal occur in volcanics both north and south of the 1954 rupture segment.

Silicification accompanies several of the alteration stages. Microfractures in igneous quartz are healed with quartz, and coarse quartz-calcite veins formed early in the sequence. Intense sericitic alteration is accompanied by an increase in the amount of quartz in the rock. Later, rock units were pervasively replaced with fine grained quartz, chalcedony, and opal.

Deep exploration wells in northern Dixie Valley crossed the Dixie Valley fault. Well data indicate that volcanic and alluvial material is altered to albite, chlorite, illite, epidote and clay. Plagioclase is altered to albite, illite, epidote, calcite and clay, and hornblende is altered to biotite, chlorite, magnetite, epidote and calcite. In the meta sediments, illite forms from andalusite, biotite alters to vermiculite and calcite. Quartz, laumontite, and adularia veins are observed (Bell et al., 1980).

#### Joint and Vein Systems

Mineral assemblages precipitated in veins and on joint surfaces occur in several sets of variably oriented fractures that formed over an extended period of time. The youngest mineral assemblages consist of prehnite-laumontite-stilbite-clay, and calcite-filled veinlets. This assemblage is concentrated in N to NE-trending fractures that parallel the Dixie Valley fault trace (Fig. 4A). Sericite-clay and older mineral assemblages are concentrated in NW to WNW-striking veins that strike at a high angle to the contemporary fault zone, and in a secondary set of NNE to NE-striking veins (Fig. 4B ). These older mineral assemblages form bands of alteration several

ten's to hundreds of meters wide that either parallel the Dixie Valley fault zone or cut into the footwall at a high angle to the fault zone (Fig. 2 and Fig. 3). Two samples of hydrothermal sericite were dated using the K/Ar method; one yielded an age of 21.8 and the other 25 ma (Table 1), indicating that this alteration occurred during Late Oligocene to Early Miocene.

The sericite-clay alteration assemblage is younger than the chlorite-epidote and biotite-K-feldspar assemblages based on cross-cutting relationships seen in the field and in thin section. The epidote-chlorite assemblage is best preserved from Little Box Canyon to Willow Creek (Fig. 3), but remnants of this assemblage extend along almost the entire length of the fault zone in the study area. In most locales along the range front, the sericite-clay assemblage overprints the epidote-chlorite mineralization. Near Sheep Creek, in the southern part of the study area (Figure 3), sericite-clay mineralization extends about 1 km into the footwall along a closely spaced set of WNW to W-striking joints and veins.

Orientations of mineral filled veins suggest that an early stage of activity on the Dixie Valley fault with an ENE to WSW extension direction is associated with mineral filled extension veins of quartz, epidote, quartz-sericite, clay minerals, and hematite. Fractures with dustings of euhedral quartz, stilbite, chlorite, calcite, epidote, and hematite are parallel to present day extension fractures.

### Fluid Inclusion Petrography

Healed microcracks in both igneous quartz and vein quartz appear as thin planar trails of numerous secondary fluid inclusions that often cross cut grain boundaries. Fluid inclusion trains cannot be traced across quartz grain boundaries where individual quartz grains are surrounded by feldspar or alteration products and are not in contact with other quartz grains. In least altered rocks there are few trains of small ( $<1\mu$ ) fluid inclusions, but most quartz grains near the fault show many intersecting planar arrays of secondary fluid inclusions. While numerous intersections of fluid inclusion trains are apparent, it is not possible to determine a fluid inclusion chronology from crosscutting relationships. Necking is a common phenomena. Fluid inclusions appear as irregular, immature to very regular mature inclusions with negative crystal shapes. Nearby fluid inclusions in linear arrays that are mature and display negative crystal outlines often have similar liquid to vapor ratios.

Fluid inclusions are categorized by their contents into: liquid+vapor, moderate salinity inclusions (type I); carbon dioxide bearing inclusions (type II); low eutectic temperature inclusions (type III); halite bearing inclusions (type IV); and one-phase (liquid) inclusions. A few inclusions contain solid phases in addition to halite. The one-phase (liquid) inclusions are the youngest.

Arrays of secondary fluid inclusions are subparallel to cataclastic veins with a second set at high angles to cataclastic veins. The orientations of fluid inclusion trails that define partly healed microfractures were measured on oriented samples of granitic rock using a universal stage (Figure 5). Poles to these trails are shown in Figure 5 contoured in terms of standard

deviations ( $\sigma$ ) from a uniform distribution of points. Three areas of high point density are apparent. The most prominent crack orientation, point density of 8-10  $\sigma$ , represents nearly vertical planes striking N38W about 15° clockwise of the dominant NW to WNW concentration of older veins observed in outcrop. The next most prominent 6-8  $\sigma$  represents planes N10W and the third set 4-6  $\sigma$  represents planes striking N72E.

The K-Ar age of hydrothermal illite in the area is 21 to 25 m.a. (Table 1) corresponding to the earlier episode of extension where the extension direction is WSW-ENE consistent with mode-I microcracks hosting fluid inclusions striking N38W. Fluid inclusion fluids on this section of the Dixie Valley fault must therefore be associated with the early phase of Basin and Range extension. The orientations of fluid inclusion trails are subperpendicular to the inferred Oligocene to Early Miocene regional stress field.

#### Fluid Inclusion Measurements

Phase changes observed in fluid inclusions on the heating-freezing microscope stage have revealed a diverse assemblage of chemically distinct fluids on the Dixie Valley fault. The thermometric measurements are summarized in Table 2. The majority of fluid inclusions measured consist of an aqueous phase and a vapor bubble usually comprising 10 to 30 volume percent (type I). Ice is the last phase to melt on warming. A second and possibly related type of inclusion contains a large vapor bubble (more than 60 volume percent) and a small volume of low salinity liquid. The presence of these two types of inclusions in close proximity to one another and showing similar homogenization temperatures, the first to liquid and the second to vapor, could be considered evidence for boiling of fluids at some stage of fault

development. However, the widespread occurrence of necked inclusions suggests that necking could also account for this association.  $\text{CO}_2$  bearing inclusions (type II) are the second type of fluid inclusion, but they are only present on some sections of the fault.

Two types of high salinity inclusions are present. A few inclusions consisting of only vapor and liquid showed eutectic temperatures well below the  $\text{NaCl-H}_2\text{O}$  eutectic (type III). The fourth type of fluid inclusions contain daughter minerals (type IV). These daughter minerals include an isometric salt probably halite, small, high relief unidentified salt, and a platy, birefringent mineral that may be sericite.

#### Moderate Salinity Inclusions (Type I)

Microthermometric measurements of fluid inclusions has revealed wide diversity in chemical composition and homogenization temperatures. Salinities in weight % NaCl equivalent calculated from ice melting temperatures are shown for 265 fluid inclusions in the histogram of Figure 6. Salinity data form a highly skewed distribution with most frequent values in the low salinity range 0 to 1% NaCl. However significant numbers of higher salinity fluid inclusions were observed.

Homogenization of most fluid inclusions occurred by disappearance of the vapor bubble. The range in homogenization temperatures is  $120^\circ$  to  $400^\circ \text{C}$  (Fig. 7). The mode of Th values is  $270^\circ\text{C}$  to  $280^\circ\text{C}$  in the southern area near Coyote and Sheep Canyon (Figure 3A) and  $180^\circ\text{C}$ - $190^\circ\text{C}$  in the Box Canyons area (Figure 3B) an area dominated by chlorite and epidote alteration (Fig. 7), although both areas have homogenization temperatures that span nearly the full range.

Homogenization temperature is plotted versus salinity for these fluid

inclusions in Figure 8a. The data points on Figure 8 indicate no apparent trends of cooling and dilution. Homogenization temperature and salinity define the fluid density and Figure 8b is contoured in terms of density. Because fluids trapped in inclusions are constant density systems, the fluids must be trapped along isochores defined by these density values.

#### Carbon Dioxide Bearing Fluid Inclusions (Type II)

Secondary fluid inclusions containing  $\text{CO}_2$  are present in several areas of the Dixie Valley fault footwall. These inclusions contain a recognizable meniscus separating liquid  $\text{CO}_2$ , vapor  $\text{CO}_2$ , and an aqueous liquid at room temperature. Thermometric properties of these inclusions are shown in Table 3. The liquid  $\text{CO}_2$  phase that is frozen by supercooling to below  $-90^\circ\text{C}$ , melts in the presence of  $\text{CO}_2$  vapor at temperatures of  $-57.6$  to  $-54.4^\circ\text{C}$ . The most frequent melting temperature is within  $0.2^\circ\text{C}$  of  $-56.6^\circ\text{C}$ , the triple point temperature of pure  $\text{CO}_2$ . Lower melting temperatures could be accounted for by small amounts of methane. The melting temperatures above  $-56.6^\circ$  can not be accounted for by any known phase equilibria, but these temperatures are reproducible and not the result of experimental error.

Clathrate melting temperatures of  $\text{CO}_2$  bearing inclusions yield salinities of 0.62 to 6.8 weight percent NaCl relative to  $\text{H}_2\text{O}$  (Table 3). These salinities together with the homogenization temperatures are plotted on Figure 8a for comparison with aqueous inclusions, but the density contours on Figure 8b apply only to the aqueous inclusions.

The  $\text{CO}_2$  component of these inclusions homogenized to liquid at  $25.4^\circ\text{C}$  to  $29.4^\circ\text{C}$  or to vapor at  $22.5^\circ\text{C}$  to  $29.3^\circ\text{C}$ . Homogenization to the liquid implies a greater density of  $\text{CO}_2$  and entrapment at higher pressure.

Overall homogenization of  $\text{CO}_2$  bearing inclusions occurred over nearly as

wide a range (197°C to 371°C) as the moderate salinity inclusions (Table 2 and Figure 8a).

#### **Inclusions with Low Eutectic Temperatures (Type III)**

Fluid inclusions with ice melting temperatures between -10.1°C and -26.0°C had very low initial melting temperatures as low as -45°C and ice crystal nucleation temperatures as low as -60°C to -80°C. These characteristics suggest the presence of a significant  $\text{CaCl}_2$  component in the fluid. These fluid inclusions have salinities of 13.6 to 25.3 weight percent  $\text{CaCl}_2 + \text{NaCl}$ . In two cases fluid inclusions were large enough and easily visible so that hydrohalite and ice melting temperatures could be observed. In these two fluid inclusions the weight fraction NaCl relative to  $\text{CaCl}_2$  was 0.3 and 0.55. Homogenization of liquid and vapor in fluid inclusions with low eutectic temperatures ranged from 120°C to 321°C. Homogenization temperatures and salinities of these inclusions are shown as open squares in Figure 8a.

#### **Inclusions Containing Halite (Type IV)**

Several fluid inclusions that contain a vapor bubble, a halite crystal and liquid at 25°C were observed. These inclusions homogenize by disappearance of the vapor bubble or by dissolution of the halite crystal. The homogenization of liquid and vapor occurred at a temperature below the halite melting temperature in several of these inclusions. Because halite melting occurred in the presence of liquid only, estimated salinity is only approximate because of the unknown slope of isopleths in P-T space (Stern et al., 1988)

Fluid inclusions with a halite daughter salt are the highest salinity fluid inclusions. Salinities determined from halite melting temperatures of

160°C to 297°C for inclusions that homogenize by vapor disappearance are 30.1 to 37.9 weight percent NaCl equivalent. In some halite bearing inclusions, however, halite was present at the temperature of vapor bubble disappearance. Some of these inclusions decrepitated before all halite had dissolved. The few halite bearing inclusions that homogenized by dissolution of halite yielded salinities of 39.2 to 43 weight percent NaCl equivalent.

#### Vapor Rich Fluid Inclusions

Inclusions in the same fluid inclusion train contained mostly vapor or liquid+vapor sometimes with halite. The vapor rich inclusions homogenized to vapor at 364° to 381° and the nearby liquid rich inclusion homogenized to liquid at 382° suggesting boiling of a high salinity fluid. However, the widespread occurrence of necked inclusions that result in varying liquid-vapor ratios suggests that necking is an alternate explanation for these vapor-rich inclusions, and that homogenization at nearly the same temperature as liquid-rich inclusions is fortuitous.

#### Discussion

The wide range in composition and homogenization temperature could be accounted for by a variety of processes. Necking of fluid inclusions could not account for the range in homogenization temperatures, because we have conscientiously avoided necked inclusions in our work.

The chemical diversity of fluid compositions on the Dixie Valley fault can be accounted for by (1) an influx of low salinity meteoric water, (2) solution of evaporites in subsurface rocks, (3) solution of present day playa evaporites in the hanging wall, (4) an influx of volcanic heated fluid, or (4) release of fluids from basement rocks at depth during dynamic rupturing.

Secondary fluid inclusions in granitic rocks often show final ice

melting temperatures in the range below the  $\text{NaCl-H}_2\text{O}$  eutectic (Konnerup-Madsen, 1977, 1979). These types of high salinity fluids are common in granitic rocks, and their occurrence in healed microfractures in the Dixie Valley fault rocks together with an intrusive age near the time of inception of Basin and Range extension suggests they may have been important fault fluids.

$\text{CaCl}_2$ - $\text{NaCl}$  brines have been observed in retrograde Ca-rich amphibolite where retrograde reactions with muscovite, epidote, and chlorite as product minerals are suggested as a mechanism for concentrating Na, K, and Ca in fluids (Crawford et al., 1979). These Ca rich compositions are most common in metamorphosed carbonate rich sediments (Roedder, 1984, p. 351). Hydrothermal Calcium chloride brines are also known from continental rift systems (Hardie, 1990).

Geothermal fluids at depth in Dixie Valley presently contain  $\text{CO}_2$ . Fluid in the deep wells contains 312 to 396 mg/l Na, 37 to 54 mg/l K, and  $\text{CO}_2$  comprises .12 to .22 wt % of the fluid (0.09 mole %) at a temperature of 206°C to 249°C (Benoit, 1989). High bicarbonate in springs emerging from igneous rocks near major faults (Bohm, 1984), vast travertine deposits at Sou hot springs, 47 km northeast of the 1954 rupture segment, and high bicarbonate (870-936 mg/l) at Hyder hot springs, 42 km north east, may be the result of  $\text{CO}_2$  leakage from a deeper geothermal reservoir.

The diversity in salinity of fluid inclusions could result from mixing of low salinity and high salinity components. These components may include cool, low salinity meteoric water, saline water formed in evaporite basins, moderate salinity thermal water, and a high temperature boiling fluid with temperature and salinity variations caused by steam separation. Lower

temperatures resulting from boiling would correspond to higher salinities as shown by the enthalpy-salinity mixing lines labeled boiling on Figure 9. Mixing of low temperature, low-salinity meteoric water with boiling fluids at any stage in their evolution towards lower T and higher salinity is labeled fresh cool water mixing on Figure 9. The present day Dixie Valley contains evaporites in Humboldt Salt Marsh and the extensive evaporites of Carson and Humboldt Sinks lie 30 km to the west.

Dixie Meadows hot springs (Figure 2) near the 1954 rupture termination consists of 35 springs and seeps over 4 square miles with wide variations in temperature and salinity. Springs emerge from alluvium in the hanging wall of the Dixie Valley fault. Temperature and salinity are inversely correlated in these springs suggesting that dissolution of evaporites by cold water and mixing with low salinity hot water accounts for the variation in temperature and salinity (Bell et al., 1980). Halite cemented breccias are present in the fault in the vicinity of the hot springs area. Saline, gypsiferous clays occur in the Truckee formation of upper Miocene age in western Nevada (Morrison, 1964). Mixing of cool, salty fluid with higher temperature, lower salinity fluids is illustrated by the trend labeled cool evaporite mixing on Figure 9. A fourth alternative is suggested by continuous displacement of the fault footwall to shallower, cooler depths. This trend is labeled isochemical cooling on Figure 9.

#### **Fluid Temperature and Pressure**

Fluid inclusion characteristics and mineral equilibria may be used to place constraints on the fluid pressure and temperature in the Dixie Valley fault footwall. Minimum pressures of entrapment are estimated from  $\text{CO}_2$  containing fluid inclusions and from inclusions containing a halite crystal.

The salinity,  $\text{CO}_2$  density, and homogenization temperatures were used together with the  $\text{CO}_2\text{-H}_2\text{O-NaCl}$  phase diagram to estimate  $\text{CO}_2$  content and minimum pressure of entrapment using the procedures of Parry (1986). Carbon dioxide content ranges from 3 to 17 mole percent, and estimated pressures on the two-phase boundary curve for inclusion compositions vary from 280 bars to 1570 bars. These pressures represent minimum entrapment pressures of a homogenous fluid. Homogenous fluids could have been trapped at higher temperatures and pressures along appropriate isochores for each fluid composition.

Roedder and Bodnar (1980) and Roedder (1984) showed that the minimum pressure of entrapment of a homogenous fluid can be estimated from halite bearing fluid inclusions by first assuming the fluid properties are adequately represented by the  $\text{NaCl-H}_2\text{O}$  system and that  $\text{NaCl}$  solubility is independent of pressure. The bulk composition of the fluid inclusion fluid and its density was estimated from the melting temperature of  $\text{NaCl}$  using the regression equation of Sterner et al. (1988). The composition and density of the saturated solution on the liquid-vapor curve at the temperature of vapor disappearance was calculated using equations from Haas (1976). At the temperature of liquid-vapor homogenization, the inclusion volume is the volume of saturated solution of known density plus the volume of halite. The mass of halite crystal is obtained from the difference in salinity at the temperature of liquid-vapor homogenization and at the temperature of  $\text{NaCl}$  melting, and its volume is calculated from halite density. These calculations yield densities of 1.137 and 1.275  $\text{g/cm}^3$  for inclusions homogenizing at the  $\text{NaCl}$  melting temperature of  $313^\circ\text{C}$  and  $356^\circ\text{C}$  respectively. Extrapolation of the density determinations of Urusova (1975) at 350 C to higher pressures

indicate a minimum entrapment pressure of about 1500 bars, but extrapolation of the MRK equation of state using the coefficients of Bowers and Helgeson indicates a pressure of 800 bars at 350°C. Extrapolation of Urusova's (1975) density measurements to 300°C yields a pressure estimate of 240 bars for the inclusion homogenizing at 313°C.

We next assume that lithostatic pressure represents a reasonable maximum and hydrostatic pressure represents a reasonable minimum for fluid pressure. Second, we infer a thermal gradient so that pressure-temperature gradients may be shown in Figure 10.

The thermal gradient on the Dixie Valley fault is probably greater than the 30°C/km gradient that is characteristic of the Basin and Range Province (Sass et al., 1981). The northern end of the belt of historic seismicity in the Central Nevada Seismic belt is an area of conspicuously high heat flow called the Battle Mountain High (Sass, et al., 1971) where thermal gradients are 40° to 50° C per km (Sass et al. 1981).

Additional indications of elevated geothermal gradients include intense hydrothermal alteration along the range front fault, fumaroles and hot water within 30 m of the surface, As and Hg in soils of the valley near the range front fault (Juncal and Bell, 1981), and hot springs widely distributed in the hanging wall of the Dixie Valley fault. The Dixie Valley geothermal area is 47 km northeast of the 1954 rupture segment where gradients of 75°C per km and above have been measured in drill holes (Bell et al., 1980) due to hydrothermal convection. These observations lend support to a thermal gradient in Dixie Valley that exceeds the normal Basin and Range gradient. Lithostatic and hydrostatic pressure gradients are shown on Figure 10 for thermal gradients of 45°C/km and 60°C/km.

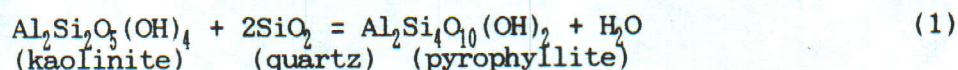
A heat source for an elevated gradient is readily available. The earliest phase of extension before 18-15 Ma was synchronous with a generally southward-migrating belt of intermediate to silicic volcanism (Sonder et al., 1987; Wernicke et al., 1987). Major Cenozoic igneous activity in the Dixie Valley area began with andesitic lava flows 35 ma (Riehle et al., 1972). Voluminous eruptions of quartz latite to rhyolite ash-flow tuffs are dated at 32 to 22 Ma (Riehle et al., 1972; Speed, 1976; Burke and McKee, 1979). Basalt flows cap the sequence and have been dated at 13 to 17 Ma (Nosker, 1981). Small igneous dikes and plutons of latite to diorite occur along the Dixie Valley fault zone. The Dixie Valley fault may be rooted within magmatic intrusion and further intrusion into the crust along the fault might allow for different subsidiary fault displacements and spreading of grabens (Thompson, 1966; Thompson and Burke, 1974; Okaya and Thompson, 1985).

The pressure and temperature of entrapment of Type I moderate salinity inclusions must lie on isochores defined by the fluid density. Fluid density is calculated from salinity and homogenization temperature measurements shown in Figures 8a and 8b. Representative isochores for densities of 0.55 to 0.95 g/cc are shown in Figure 10 corresponding to densities of one wt.% NaCl solutions that homogenize by vapor disappearance at various temperatures. These fluids would have been trapped along their respective isochores at pressures and temperatures between lithostatic and hydrostatic pressures.

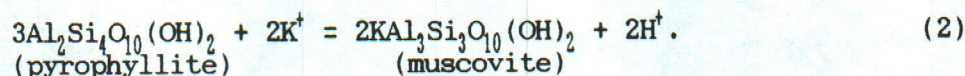
The minimum pressure and temperatures of entrapment of type II,  $\text{CO}_2$  bearing inclusions is shown on Figure 10. These fluids, too, would have been trapped on isochores defined by the density of the fluid. The wide range in minimum pressures of entrapment has been interpreted to be the result of pressure transients accompanying dilatant fracturing (Parry and Bruhn, 1990).

The highest pressure values are near lithostatic pressure, and the lowest are near hydrostatic pressure.

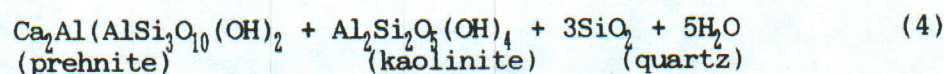
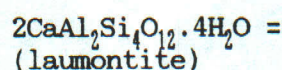
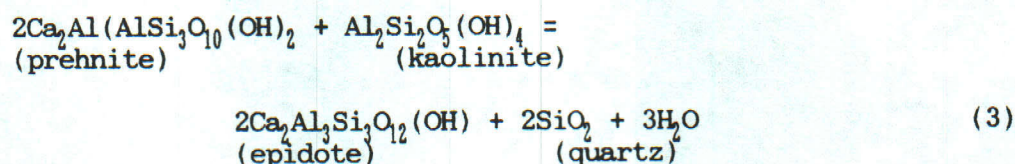
Additional constraints are placed on P-T conditions by mineral equilibria. Equilibria among kaolinite, pyrophyllite, quartz, and water according to reaction (1)

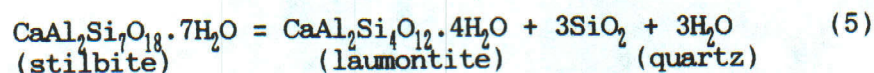


shown on Figure 10 indicates that the presence of kaolinite in these quartz rich rocks requires temperatures below about 270 C. Pyrophyllite has not been observed despite numerous fluid inclusion homogenization temperatures that exceed 270°C. The reason for this is that fluids contain sufficient K<sup>+</sup> to stabilize muscovite according to reaction (2).



The low-temperature stability of epidote in the presence of quartz and an aqueous solution at pressures between 500 and 3800 bars is represented by reaction (3) (Bird and Helgeson, 1981). Prehnite is stable relative to laumontite above about 220°C (reaction (4)) and stilbite is stable relative to laumontite below about 130°C to 140°C at pressures below 600 bars (reaction (5)).





Examination of these equilibria on Figure 10 shows that mineral assemblages along with fluid inclusion properties record a systematic decrease in both temperature and pressure with displacement of the footwall during faulting. Fluid temperature at depth on the fault exceeded 350°C and pressure exceeded 1500 bars. K-feldspar, biotite, epidote, chlorite, and muscovite were the earliest formed stable mineral phases. As temperature and pressure decreased, kaolinite was stabilized relative to muscovite and pyrophyllite below about 270°C, prehnite was stabilized relative to epidote and then laumontite was stabilized relative to prehnite at about 220°C. At 140°C stilbite is stable relative to laumontite and the fluid pressure must be lower than 600 bars, otherwise heulandite would occur. As pressure and temperature decreased, CO<sub>2</sub> separated so that zeolites were stabilized relative to calcite and clay.

#### Regional Implications

Regional extension in the great Basin dates from about 30 Ma and occurred in two episodes. The extension direction in northern Nevada changed by clockwise rotation of 45 degrees from WSW-ENE (S68W-N68E) at about 10Ma to the present day extension direction of N65W-S65E (Zoback et al, 1981; Zoback and Thompson, 1978; Eaton, 1982). The early phase of extension dated at 23-15 Ma based on angular unconformity and rotated high angle faults (John et al., 1989) was accommodated by rotation of crustal blocks, strike slip motion on northwest trending faults, and normal faults that predate widespread basaltic volcanism dated at 13 to 17 Ma (Hudson and Geisman, 1987). The later episode of extension beginning at 10 to 13 Ma (Eddington et al., 1987; Zoback et al., 1981) is indicated by 10 Ma old basalt on the west flank of Job

Peak that is tilted  $10^{\circ}$  west (Wallace and Whitney, 1984)

The orientation and age of hydrothermal minerals in the older, NW to WNW trending vein arrays indicate that these features probably reflect Oligocene to Early Miocene deformation and hydrothermal activity, which occurred prior to the onset of NNE-trending Basin and Range normal faulting (Stewart et al., 1977). The Stillwater Range lies in part of a regional WNW-trending belt of mostly silicic volcanism that extended across southern Nevada from Late Eocene through Early Miocene time. This belt was characterized by widespread hydrothermal alteration and NW to WNW-trending structural trends that included numerous dikes, caldera complexes, and high-angle fault and joint systems (Boden, 1986). In some locales, NE-trending faults formed as subsidiary features (Rielhe et al., 1972; Boden, 1986; Hudson and Geissman, 1987). Hudson and Geissman (1987) noted that clockwise rotation of rocks in the central Stillwater Range and Clan Alpine Mountains occurred as the result of movement on a complex array of strike-slip, oblique-slip, and dip-slip faults and suggested that rotation was accompanied mostly movement on NW-striking, right-lateral faults. Remnants of this fault set were preserved in the interior of the Stillwater Range near White Rock Canyon and Coyote Canyon, and may be represented by the western fault branch in the "Bend", within the present-day Dixie Valley fault zone (Fig.11).

Basalt and andesite caps the range at an elevation of 2200 m and also produces seismic reflections in Dixie valley at an elevation 1280 m below sea level for a total of post 13-17 Ma displacement on the fault of 3.5 km (Wallace and Whitney, 1984) to 2.2 km further north (Okaya and Thompson, 1985). This displacement estimate includes only post 13 to 17 Ma displacement. Hydrothermal activity and tectonic displacement on the Dixie Valley fault

began earlier. K/Ar ages of hydrothermal sericite on the fault are 21.8 to 25 Ma (Table 1) and mineral filled veins and fluid inclusion train orientations are consistent with the earlier extension direction. Total displacement likely exceeds the post 13 to 17 Ma displacement estimates. Moderate salinity fluid inclusions would have been trapped at the pressure and temperature defined by the isochore for the fluid density illustrated on Figure 10. Fluid inclusions containing  $\text{CO}_2$  were trapped at minimum pressures as high as 1570 bars at a temperature of  $305^\circ\text{C}$  (Table 3) shown in Figure 10 and corresponding to a lithostatic pressure at a depth of over 6 km. Aqueous fluid inclusions that homogenize at  $380^\circ$  to  $400^\circ\text{C}$  then if trapped no deeper than 6 km must have been trapped at a thermal gradient of nearly  $70^\circ\text{C}/\text{km}$ .

Evidence suggest that the present-day Dixie Valley fault zone began to form during Oligocene to Early Miocene time, and may have undergone two phases of extension. First, the fact that sericite-clay and older alteration mineral assemblages occur in a narrow band along the present-day fault trace suggests that a zone of intense fracturing and hydrothermal alteration with a geometry roughly similar to that of the Quaternary fault zone formed during Oligocene to Early Miocene time. Secondly, paleo-fluid entrapment pressures estimated from measurements of high-temperature fluid inclusions indicate a minimum footwall uplift of 6 km. This is 3 to 4 km more vertical displacement than the post 13-17 Ma displacement estimate of 3.5 to 2.2 km (Wallace and Whitney, 1984; Okaya and Thompson, 1985), suggesting that the early phase of vertical displacement was similar in magnitude to that of the later phase. Notably, the post 13-17 Ma displacement is estimated from offset of basalts that were extruded over a fairly flat surface. A period of tectonic quiescence must have occurred between the early and later phases of extension across the Dixie

Valley fault zone. Thirdly, we note that the Dixie Valley fault trace is highly sinuous, with two strong maxima in fault strike, one towards the WNW to NNW and the other NNE to NE (Figure 11). Perhaps this pattern is partly inherited from the earlier, Oligocene to Early Miocene phase of extension, when deformation was concentrated on WNW-striking strike-slip faults and subsidiary normal and normal-oblique-slip faults, many of which trended NNE to NE, forming a rectangular fault pattern when observed in map view (Riehle et al., 1972; Hudson and Geissman, 1987; Boden, 1986). The NNW-trending fault that forms the western branch of the Dixie Valley fault zone in the area of The Bend may be the largest example of a partly reactivated Oligocene to Early Miocene fault in the study area. Presumably, rotation of extension from N68E to S65E about 10 ma ago enhanced movement on NNE to NE-trending normal faults, relative to older sets of WNW to NNW-trending faults. Never-the-less, the distribution of hydrothermal alteration minerals, and the internal structure of the Dixie Valley fault zone indicate that much of the overall structural geometry is inherited from Oligocene and Early Miocene deformation and hydrothermal circulation.

The regional extension axis was oriented about N68E during Oligocene to Early Miocene (Zoback et al. 1981) and was sub-perpendicular to the WNW to NW-striking veins and healed microfractures in the footwall of the Dixie Valley fault zone. Therefore, many fluid inclusion measurements reported in this study may reflect temperature, composition and fluid pressures during this older phase of faulting, rather than during the Late Miocene to Recent period of Basin and Range normal faulting. The higher fluid pressures and temperatures, and the alteration minerals K-feldspar, biotite, chlorite, epidote, and muscovite date from this older faulting episode.

### Comparisons with Contemporary Faults

Two well-studied contemporary fault systems in the Great Basin provide valuable comparisons. The Wasatch Fault in the eastern Great Basin (Parry and Bruhn, 1986; Parry et al., 1988) and the Nevada Comstock fault in western Nevada (Vikre, 1989) are normal faults with displacement histories beginning in the Miocene.

Exhumation of the footwall of the southern end of the Salt Lake segment of the Wasatch fault has exposed hydrothermally altered granitic rocks. Vein filling and pervasive alteration mineralogy includes, from earliest to latest, biotite-K-feldspar, chlorite-epidote-sericite, and laumontite-prehnite-clay. Secondary fluid inclusions present in healed fractures in quartz associated with syntectonic chlorite-epidote-sericite alteration contain 3 to 32 mole %  $\text{CO}_2$  with 4.5 to 17.3 weight % NaCl solution. The mode of homogenization temperatures is  $285^\circ\text{C}$ . Estimated minimum entrapment pressures vary from 600 bars to 2950 bars. The mode of homogenization temperatures of secondary inclusions associated with the later laumontite-prehnite assemblage is  $100^\circ\text{C}$ , salinity ranges from 2.0 to 16.0 wt. % NaCl equivalent, and no  $\text{CO}_2$  was detected.

Fluid pressure and temperature evolved along a path from lithostatic to hydrostatic with continued displacement of the footwall relative to the hanging wall. Age constraints are provided by a  $17.6 \pm 0.6$  m.y. K-Ar age of hydrothermal sericite from a sample with mean  $T_h$  of  $309^\circ\text{C}$ , and 7.3 to 9.6 m.y. fission track ages of apatite (closure temperature  $120 \pm 15^\circ\text{C}$ ). Temperature and pressure estimates suggest post 17.6 Ma fault displacement is 11 km at a thermal gradient of  $30^\circ\text{C/km}$  (Parry and Bruhn, 1987).

The major tectonic consequence of the pore fluid and chemical reactions

observed on the Wasatch fault is reduction of effective stress by pore fluid pressure. Elevated pressures are enhanced by chemical reactions that seal the tectonically induced cracks in the rock. The mechanical behavior of the rock is also modified by formation of chlorite and sericite with epidote in the fault rock at deeper levels, and vein fillings of zeolite, calcite, and clay minerals at shallower levels.

A contemporary fault system that has been examined in detail due to bonanza economic mineralization, the Comstock fault at Virginia City Nevada, shows many similarities to the Dixie Valley fault. The Comstock fault is a major mineralized crustal structure 135 km southwest of Dixie Valley. This fault displaces Miocene volcanic rocks 762 to 1219 meters (Vikre et al., 1988) and is mineralized over 4.6 km of strike length and to 1000 meters below the present surface. Post Miocene displacement is less than 183 m and the fault is not presently active. Fault-related alteration and fluid characteristics date from the earlier episode of Basin and Range extension without superimposition of younger hydrothermal events. Alteration which is associated with precious metal veins and the Comstock fault includes strong silicification adjacent to the Comstock Fault with accompanying sericite, chlorite and pyrite. Near lode margins quartz, sericite, chlorite, montmorillonite, and pyrite overlie quartz + sulfide lodes. K-feldspar, albite, sericite, chlorite, and calcite locally occur with sulfides.

Alteration not related to the fault includes chlorite, calcite, epidote, albite, quartz and pyrite that comprise a propylitic assemblage with no close association the Comstock fault; a younger albite, natrolite, stilbite assemblage; and an assemblage of quartz, alunite, pyrophyllite, clay.

Fluids circulated at least 2000 m below the Miocene paleosurface at

temperatures from  $>300^{\circ}\text{C}$  to  $>235^{\circ}\text{C}$ , with salinities of  $<1$  to  $>6\%$  NaCl and up to  $2.1\text{ Wt } \%$   $\text{CO}_2$ . Fluids with recognizable  $\text{CO}_2$  contain  $<3.2\%$  NaCl, fluids with no  $\text{CO}_2$  contain  $0.4$  to  $6.1\%$  NaCl and fluid inclusions with daughter NaCl and KCl contain  $23\%$  NaCl and  $47\%$  KCl. Boiling and mixing were invoked by Vikre (1989) to account for variable solution compositions, but the  $\text{CO}_2$  bearing inclusions were determined to be later than those with no  $\text{CO}_2$ .

### Conclusions

Detailed mapping, petrographic, and fluid inclusion work on the Dixie Valley fault and comparison with the Wasatch fault and Comstock fault suggests a model for Basin and Range seismogenic faults from which the relationship of fault behavior to fluid characteristics can be derived.

Hydrothermally altered footwall rocks have been exhumed by fault displacement and erosion on the Dixie Valley Fault, Nevada. Much of the footwall of the 1954 rupture segment consists of Tertiary age granitic rocks that provide aluminosilicate parent minerals for the alteration and constrain the maximum age of the alteration to less than 28 Ma. Overlapping episodes of hydrothermal mineral formation were produced as displacement of the fault progressed. These minerals are from earliest to latest: hydrothermal biotite+K-feldspar, chlorite+epidote, sericite+kaolinite+smectite, prehnite+laumontite+stilbite+clay, and chalcedony, opal, smectite, alunite, and kaolinite. Microthermometric measurement of fluid inclusion characteristics indicate a diverse fluid chemistry, temperature, and pressure of entrapment. Hydrothermal alteration minerals and characteristics of secondary fluid inclusions trapped in healed microfractures in igneous quartz place constraints on fluid pressure and temperature during faulting.

Fluid inclusions in hydrothermally altered footwall rocks of the Dixie

Valley fault, Nevada and the Wasatch fault, Utah indicate that pore fluid pressure fluctuated from 1570 to 350 bars in the temperature range 350° to 200°C. Scatter in the pressure estimates at constant temperature is interpreted as paleo-fluid pressure transients at depths of up to 3 to 5 km on the Dixie Valley fault. The pressure transients are greatest on both faults in the temperature range 270 to 310 C.

Interaction of the pore fluid with host rock quartz monzonite on the Dixie Valley fault has resulted in a series of temperature dependent chemical reactions producing minerals that seal fractures and alter the mechanical properties of the rock. Ductile deformation combined with hydrothermal crack sealing must effectively prevent fluid communication with near surface fluids. As deformation becomes more brittle, rock fractures are less effectively sealed and fluid pressures drop to hydrostatic conditions. Upward displacement of footwall rocks and decreasing fluid pressure permit open system conditions, effervescence of  $\text{CO}_2$ , and precipitation of calcite, zeolite, and other minerals in rock fractures.

Fault domains at a depth of up to 5 km on the Dixie Valley fault containing a  $\text{CO}_2$ -rich fluid may play a key role in nucleation and propagation of earthquake ruptures. Ruptures may be initiated by high pore pressures caused by porosity reduction. New pore volume produced by dilatancy coupled with low rock permeability then results in decompression of the fluid that may stabilize rupture by dilatant hardening. Separation of  $\text{CO}_2$ - $\text{H}_2\text{O}$ - $\text{NaCl}$  fluids into two phases results in a drastic reduction in fluid bulk modulus that diminishes the dilatant hardening effect and permits ruptures to propagate. The Dixie Valley fault fluids and alteration show many similarities to fluids on the Wasatch fault, Utah and the Comstock fault, Nevada.

### Acknowledgments

Financial support provided by NSF Grant EAR-8618250 to RLB and WTP. The manuscript was carefully reviewed by Paula N. Wilson and Ricardo Presnell.

### Bibliography

---

Anderson, R. E., Zoback, M. L., and Thompson, G. A., Implications of selected subsurface data on the structural form and evolution of some basins in the northern Basin and Range province, Nevada and Utah, Geological Society of America Bulletin 94, 1055-1072, 1983.

Bateman, R. L., and Hess, J. W., Hydrologic inventory and evaluation of Nevada playas, Project report No. 49, Water Resources Center, Desert Research Institute, University of Nevada, Las Vegas 137 pp., 1978.

Bell, E. J., Campana, M. E., Jacobson, R. L., Larson, L. T., Slemmons, D. B., Bard, T. R., Bohm, B. W., Ingraham, N. L., Juncal, R. W., and Whitney, R. A., Geothermal reservoir assessment case study, northern Basin and Range province, northern Dixie Valley, Nevada, Report, Mackay Minerals Research Institute, University of Nevada, Reno, Nevada, 223 pp., 1980.

Bell, J. W. and Katzer, T., Surficial geology, hydrology, and late Quaternary tectonics of the IXL Canyon area, Nevada, Nevada Bureau of Mines and Geology Bulletin 102, University of Nevada-Reno, 51 pp., 1987.

Bell, J. W. and Katzer, T., Timing of late Quaternary faulting in the 1954 Dixie Valley earthquake area, central Nevada, Geology, 18, 622-625., 1990.

Benoit, W. R., Carbonate scaling characteristics in Dixie Valley, Nevada geothermal wellbores, Geothermics 18, 41-48, 1989.

Bird D. K., and Helgeson H. C., Chemical interaction of aqueous solutions with epidote-feldspar mineral assemblages in geologic systems. II. Equilibrium constraints in metamorphic/geothermal processes, Amer. J. Sci. 281, 576-614, 1981.

Boden, D. R., Eruptive history and structural development of the Toquima caldera complex, central Nevada, Geological Society of America Bulletin, 97, 61-74, 1986.

Bodnar R. J., Reynolds T. J., and Kuehn C. A., Fluid-inclusion systematics in epithermal systems. in Geology and Geochemistry of Epithermal Systems (eds. B. R. Berger, and P. M. Bethke) Reviews in Economic Geology, Vol. 2, pp. 73-97. Soc. Econ. Geol., 1985.

Bohm, B., Possible relations between anomalous spring water chemistry in the Stillwater Range, and the Dixie Valley Geothermal system, Northern Nevada, Geothermal Resources Council Transactions vol. 8, 369-371, 1984.

Bowers T. S. and Helgeson H. C., Calculation of the thermodynamic and geochemical consequences of nonideal mixing in the system  $H_2O-CO_2-NaCl$  on phase relations in geologic systems: Equation of state for  $H_2O-CO_2-NaCl$  fluids at high pressures and temperatures, Geochim. Cosmochim. Acta 47, 1247-1275, 1983.

Bozzo A. T., Chen H-S., Kass J. R., and Barduhn A. J., The properties of the hydrates of chlorine and carbon dioxide, Desalination 16, 303-320, 1975.

Burke, D. B., and McKee, E. H., Mid-Cenozoic volcano-tectonic troughs in central Nevada, Geological Society of America Bulletin, 90, 181-184, 1979.

Cho, M., Maruyama, S. and Liou, J. G., An experimental investigation of heulandite-laumontite equilibrium at 1000 to 2000 bar Pfluid, Contrib. Mineral. Petrol. 97, 43-50, 1987.

Collins P. L. F., Gas hydrates in CO<sub>2</sub>-bearing fluid inclusions and the use of freezing for estimation of salinity, Econ. Geol., 74, 1435-1444, 1979.

Crawford, M. L., Filer, J. and Wood, C., Saline fluid inclusions associated with retrograde metamorphism, Bull. Mineral. 102, 562-568, 1979.

Eaton, G. P., The Basin and Range province: origin and tectonic significance, Ann. Rev. Earth and Planet. Sci, 10, 409-440, 1982.

Eddington, P. K., Smith, R. B. and Renggli, C., Kinematics of Basin and Range intraplate extension, in Coward, M. P., Dewey, J. F. and Hancock, P. L. eds Continental extensional tectonics, Geological Society Special Publication No. 28, p. 371-392, 1987.

Haas, J. L., Jr., Physical properties of the coexisting phases and thermochemical properties of the H<sub>2</sub>O component in boiling NaCl solutions, U. S. Geol. Surv. Bull. 1421-A, 73 pp., 1976.

Hardie, L. A., The roles of rifting and hydrothermal CaCl<sub>2</sub> brines in the

origin of potash evaporites. An Hypothesis, Am. Jour. Sci., 290, 43-106, 1990.

Hemley, J. H., Montoya, J. W., Marinenko, J. W. and Luce, R. W., Equilibria in the system  $\text{Al}_2\text{O}_3$ - $\text{SiO}_2$ - $\text{H}_2\text{O}$  and some general implications for alteration/mineralization processes, Econ. Geol. 75, 210-228, 1980.

Hubbert, M. K. and Rubey, W. W., Role of fluid pressure in the mechanics of overthrust faulting, Geological Society of America Bulletin, 70, 115-205, 1959.

Hudson, M. R. and Geissman, J. W., Paleomagnetic and structural evidence for middle Tertiary counterclockwise block rotation in the Dixie Valley region, west-central Nevada, Geology, 15, 638-642, 1987.

Ismail, I. A. H. and Murrell, S. A. F., Dilatancy and the strength of rocks containing pore water under undrained conditions. Geophys, J. R. Astr. Soc., 44: 107-136, 1976.

Janecke, S. U. and Evans, J. P., Feldspar-influenced rock rheologies: Geology, 16, 1064-1067, 1988.

John, D. A., Thomason, R. E., and McKee, E. H., Geology and K-Ar geochronology of the Paradise Peak mine and the relationship of pre-Basin and Range extension to early Miocene precious metal mineralization in west central Nevada, Econ. Geol. 84, 631-649, 1989.

Juncal, R. W., and Bell, E. J., Solid-sample geochemistry study of western Dixie Valley, Churchill County, Nevada--Part II, Soil Geochemistry, Geothermal Resources Council Transactions Vol 5, 51-54, 1981.

Kamb, W. B., Petrofabric observations from Blue Glacier, Washington, in relation to theory and experiment, J. Geophys. Res. 64, 1891-1909, 1959.

Kirby, S. H. and Kronenberg, A. K., Rheology of the lithosphere: selected topics: Reviews in Geophysics, 25, 1219-1244, 1987.

Konnerup-Madsen, J., Composition and microthermometry of fluid inclusions in the Kleivan granite, south Norway, Am. Jour. Sci. 277, 673-696, 1977.

Konnerup-Madsen, J., Fluid inclusions in quartz from deep-seated granitic intrusions, south Norway, Lithos 12, 13-23, 1979.

Liou, J. G., Stilbite-laumontite equilibrium, Contr. Mineral. and Petrol., 31, 171-177, 1971.

Meister, L. J., Seismic refraction study of Dixie Valley, Nevada, Ph. D. thesis, Stanford University, 72 pp., 1967.

Morrison, R. B., Lake Lahontan: Geology of the southern Carson Desert, Nevada, U. S. Geol. Survey Professional Paper 401, 156 p., 1964.

Nosker, S. A., Stratigraphy and structure of the Sou Hills, Pershing County,

Nevada, M. S. Thesis, Reno, University of Nevada, 60p., 1981.

Oakes, C. S., Bodnar, R. J., and Simonson, J. M., The system  $\text{NaCl}-\text{CaCl}_2-\text{H}_2\text{O}$ :  
I. The ice liquidus at 1 atm total pressure, *Geochim. Cosmochim. Acta.* 54,  
603-610, 1990.

Okaya, D. A. and Thompson, G. A., Geometry of Cenozoic extensional faulting:  
Dixie Valley, Nevada, *Tectonics*, 4, 107-125, 1985.

Page, Ben M., Preliminary geologic map of a part of the Stillwater Range,  
Churchill County, Nevada, Nevada Bureau of Mines and Geology, Map 28, 1965.

Parry W. T., Estimation of  $X_{\text{CO}_2}$ , P, and fluid inclusion volume from fluid  
inclusion temperature measurements in the system  $\text{NaCl}-\text{CO}_2-\text{H}_2\text{O}$ . *Econ. Geol.*,  
81, 1009-1013, 1986.

Parry W. T., and Bruhn R. L., Pore fluid and seismogenic characteristics of  
fault rock at depth on the Wasatch fault, Utah. *J. Geophys. Res.*, 91, 730-  
744, 1986.

Parry W. T., and Bruhn R. L., Fluid inclusion evidence for minimum 11 km  
vertical offset on the Wasatch fault, Utah. *Geology*, 15, 67-70, 1987.

Parry, W. T., Wilson, P. N. and Bruhn, R. L., Pore-fluid chemistry and  
chemical reactions on the Wasatch normal fault, Utah. *Geochimica et*  
*Cosmochimica Acta*, 52, 2053-2063, 1988.

Parry, W. T., and Bruhn, R. L., Fluid pressure transients on seismogenic normal faults, *Tectonophysics*, 179, 335-344, 1990.

Potter R. W., II, and Brown D. L., The volumetric properties of aqueous sodium chloride solutions from 0°C to 500°C at pressures up to 2000 bars based on regression of available data in the literature, U. S. Geol. Surv. Bull. 1421-C, 36pp, 1977.

Potter R. W. II, Clyne M. A., and Brown D. L., Freezing point depression of aqueous sodium chloride solutions, *Econ. Geol.* 73, 284-285, 1978.

Riehle, J. R., McKee, E. H. and Speed, R. C., Tertiary volcanic center, west-central Nevada, *Geological Society of America Bulletin*, v. 83, p. 1383-1396, 1972.

Roedder E., *Fluid Inclusions*, Reviews in Mineral. vol. 12, Mineral. Soc. Amer. 644pp, 1984.

Roedder E. and Bodnar, R. J., Geologic pressure determinations from fluid inclusion studies. *Ann. Rev. Earth Planet Sci.*, 8, 263-301, 1980.

Roeloffs, E., and Rudnicki, J. W., Coupled-deformation diffusion effects on water level changes due to propagating creep events. *Pure Appl. Geophys.*, 122, 560-582, 1985.

Rudnicki, J. W. and Chen C. J., Stabilization of rapid frictional slip on a weakening fault by dilatant hardening, *Geophys. Res.* 93, 4745-4757, 1988.

Sass, J. H., Lachenbruch, A. H., Monroe, R. H., Greene, G. W., and Moses, T. J., Jr., Heat flow in the western United States, *Jour. Geophys. Res.* 76, 6376-6413, 1971.

Sass, J. H., Blackwell, D. D., Chapman, D. S., Costain, J. K., Decker, E. R., Lawver, L. A., and Swanberg, C. A., Heat flow from the crust of the United States, In Touloukian, Y. S., Judd, W. R., and Roy, R. F. (Editors), *Physical Properties of Rocks and Minerals, McGraw-Hill/CINDAS Data Series on Material Properties Volume II-2*, p5681-5698, 1981.

Sibson R. H., Controls on low-stress hydro-fracture dilatancy in thrust, wrench and normal fault terrains, *Nature* 289, 665-667, 1981.

Sibson, R. H., Fluid flow accompanying faulting: field evidence and models, in *Earthquake prediction: an International Review* (eds. Simpson, D. W., and Richards, P. G.) 593-603 (Maurice Ewing Series 4, AGU, Washington D. C., 1981.

Sibson, R. H., Robert, F., and Poulson, K. H., High-angle reverse faults, fluid-pressure cycling, and mesothermal gold-quartz deposits, *Geology*, 16, p. 551-555, 1988.

Sonder, L. J., England, P. C. Wernicke, B. P., and Christiansen, R. L., 1987, A physical model for Cenozoic extension of western North America in Coward, M.

P., Dewey, J. F., and Hancock, P. L., eds, Continental Extensional Tectonics, Geological Society (London) Special Publication 28, 187-201, 1987.

Speed, R. C., Geologic map of the Humboldt Lopolith, Geological Society of America Map and Chart Series MC-14, Scale 1:81050, 1976.

Speed, R. C. and Armstrong, R. L., Potassium-Argon ages of some minerals from igneous rocks of western Nevada, Isochron/West, 71-1, 1-8, 1971.

Sterner S. M., and Bodnar R. J., Synthetic fluid inclusions in natural quartz I. Compositional types synthesized and applications to experimental geochemistry, Geochim. Cosmochim. Acta 48, 2659-2668, 1984.

Sterner, S. M., Hall, D. L., and Bodnar, R. J., Synthetic fluid inclusions V. Solubility relations in the system NaCl-KCl-H<sub>2</sub>O under vapor saturated conditions, Geochim. Cosmochim. Acta 52, 989-1005, 1988.

Stewart, J. H., Geology of Nevada, Nevada Bureau of Mines and Geology Special Publication 4, 136 p., 1980.

Stewart, J. H., Moore, W. J. and Zeitz, I., East-west patterns of Cenozoic igneous rocks, aeromagnetic anomalies, and mineral deposits, Nevada and Utah, Geological Society of America Bulletin, v. 88, p. 67-77, 1977.

Thenhaus, P. C. and Barnhard, T. P., Regional termination and segmentation of Quaternary fault belts in the Great Basin, Nevada and Utah, Bull. Seis. Soc.

Am., 79, 1426-1438, 1989.

Thompson A. B.,  $\text{PCO}_2$  in low-grade metamorphism; zeolite, carbonate, clay mineral, prehnite relations in the system  $\text{CaO}-\text{Al}_2\text{O}_3-\text{SiO}_2-\text{CO}_2-\text{H}_2\text{O}$ , Contrib. Mineral. Petrol., 33, 145-161, 1971.

Thompson, G. A., The rift system of the western United States, in The World Rift system ed. T. N. Irvine. Geol. Surv. Canada Dept. Mines Tech Surv. Pap. 66-14, 280-290, 1966.

Thompson, G. A., Perspective from the Fairview Peak - Dixie Valley Earthquakes of 1954, Proceedings of USGS workshop on the Borah Peak Earthquake, USGS Open File Report, 1984.

Thompson, G. A. and Burke, D. B., Rate and direction of spreading in Dixie Valley, Basin and Range province, Nevada, Geol. Soc. Am. Bull. 84, 627-632, 1973.

Thompson, G. A. and Burke, D. B., Regional geophysics of the Basin and Range province, Annu. Rev. Earth and Planet. Sciences 2, 213-238, 1974.

Urusova, M. A., Volume properties of aqueous solutions of sodium chloride at elevated temperatures and pressures, Russian Journal of Inorganic Chemistry v. 20, p. 1717-1721, 1975.

Vanko, D. A., Bodnar, R. J. and Sterner, S. M., Synthetic fluid inclusions:

VIII. Vapor saturated halite solubility in part of the system  $\text{NaCl}-\text{CaCl}_2-\text{H}_2\text{O}$ , with application to fluid inclusions from oceanic hydrothermal systems, *Geochim. Cosmochim. Acta*, 52, 2451-2456, 1988.

Vikre, P. G., Fluid-mineral relations in the Comstock lode, *Econ. Geol.* 84, 1574-1613, 1989.

Vikre, P. G., McKee, E. H., and Silberman, M. L., Chronology of Miocene hydrothermal and igneous events in the western Virginia Range, Washoe, Storey, and Lyon Counties, Nevada, *Econ. Geol.* 83, 864-874, 1988.

Wallace, R. E., Patterns and timing of late Quaternary faulting in the Great Basin province and relation to some regional tectonic features, *J. Geophys. Res.* 89, 5763-5769, 1984.

Wallace, R. E. and Whitney, R. A., Late Quaternary history of the Stillwater seismic gap, Nevada. *Bull. Seis. Soc. Am.*, 74, 301-314, 1984.

Wernicke, B. P., Christiansen, R. L., England, P. C., and Sonder, L. J., Tectonomagmatic evolution of Cenozoic extension in the North American Cordillera in Coward, M. P., Dewey, J. F. and Hancock, P. L. eds, *Continental Extensional Tectonics*, Geological Society (London) Special Publication No. 28, pp. 203-221, 1987.

Willden, R. and Speed R. C., Geology and mineral resources of Churchill County, Nevada, *Nevada Bureau of Mines and Geology Bulletin* 83, 95 pp, 1974.

Zoback, M. L., and Thompson, G. A., Basin and Range rifting in northern Nevada: clues from a mid-Miocene rift and its subsequent offsets, *Geology*, 6, 111-116, 1978.

Zoback, M. L. Anderson, R. E. and Thompson, G. A., Cainozoic evolution of the state of stress and style of tectonism of the Basin and Range province of the western United States, *Phil. Trans. Royal Soc. London* 300, 407-34 Series A, 1981.

## FIGURE CAPTIONS

Figure 1. Index map of Nevada showing the Stillwater Mountain Range. Square indicates the portion of the range and Dixie Valley shown in Figure 2.

Figure 2. Generalized geologic map of a portion of the Stillwater Mountain range modified from Page (1965). The range front fault is shown as a heavy line. A, B, and C are sections of the Dixie Valley fault and footwall shown in detail in Figure 3.

Figure 3. Geologic, alteration, and sample location map of portions of the Dixie Valley fault. Temporally and spatially overlapping hydrothermal alteration mineral assemblages in footwall rocks are shown. A--= Coyote Canyon area, B--Box Canyon Area, C--IXL canyon area.

Figure 4. A. Rose diagram of strike directions of open fractures on the Dixie Valley fault, Nevada. B. Rose diagram of strike directions of hydrothermal veins.

Figure 5. Equal area stereographic plot of poles to fluid inclusion trails, lower hemisphere. Contoured in terms of standard deviations from a uniform distribution of points (Kamb, 1959) with the contour interval of 2 sigma indicated by width of ruled lines. A uniform distribution is represented by 3 sigma, so the unruled area representing 2-4 sigma represents the area of the diagram in which the counting circle contained a distribution of points equivalent to 1 sigma on either side of the density of a uniform distribution of points.

Figure 6. Histogram of salinities of Type I and Type III fluid inclusions calculated from ice melting temperatures using the regression equation of Potter et al. (1978).

Figure 7. A. Homogenization temperatures of aqueous fluid inclusions from the Dixie Valley fault footwall. B. Homogenization temperatures of fluid inclusions from the Coyote Canyon area of Figure 3A. C. Homogenization temperatures of fluid inclusions from the Box Canyons area (Figure 3B, and 3C).

Figure 8a. Temperature of homogenization of fluid inclusions plotted versus salinity. Symbols are open squares, low eutectic inclusions; open circles,  $\text{CO}_2$  inclusions; solid circles, aqueous inclusions. Figure 7b. Aqueous inclusions contoured in terms of density using the equations and coefficients of Potter and Brown (1977). Density contours do not apply to  $\text{CO}_2$  inclusions shown as open circles.

Figure 9. Hypothetical mixing models for fluids on the Dixie Valley fault.

Figure 10. Minimum pressure and temperature for entrapment of  $\text{CO}_2$  fluid inclusions (solid circles), lithostatic and hydrostatic pressure gradients, mineral equilibria, and boiling curves. K, kaolinite; P, pyrophyllite; Q, quartz; W, water; L, laumontite; Pr, prehnite; S, stilbite; H, heulandite. Data for reactions:  $\text{K}+\text{Q}=\text{P}+\text{W}$  from Hemley et al. (1980);  $\text{L}=\text{Pr}+\text{K}+3\text{Q}+5\text{W}$  from Bird and Helgeson (1981);  $\text{S}=\text{H}+\text{W}$  and  $\text{H}=\text{L}+3\text{Q}+2\text{W}$  from Cho et al. (1987); and  $\text{S}=\text{L}+3\text{Q}+3\text{W}$  from Liou (1971). Isochores calculated for 1% NaCl solution and various

homogenization temperatures from data of Potter and Brown (1977). Boiling curve calculation used data and equations of Haas (1976).

Figure 11. A. Map view of the rupture trace of the Dixie Valley fault. Localities referred to in the text are 1. White Rock Canyon; 2. The Bend; and 3. Coyote Canyon. B. Map view of proposed development of the Dixie Valley fault from superposition of faults developed in contemporary stress field on Oligocene to Late Miocene faults.

Table 1. Potassium-Argon age data.

Map No.	Sample	Description	Locality	Dated Mineral	K wt%	40Ar*/40Ar total%	40Ar* x10 <sup>-10</sup> mol/g	Age Ma±sigma
108	IXL Pluton	Fine to coarse plag K-feldspar, quartz	30°41'27"N 118°08'02"W	Biotite	6.91	69	3.40	28±2.0
D	DV87-59	Very coarse Muscovite + quartz vein in granite		Muscovite	8.91	82.1 89.7	12.37	78.4±2.9
18	DV87-7	Sericite completely replacing feldspars in granite		Muscovite	7.72	26.5 35.3	3.37	25.0±1
20	DV87-5b	Near quantitative replacement of feldspars in granite		Muscovite	7.07	54.6	2.69	21.8±0.9

Analyses by Geochron Laboratories  
 $\lambda_{\text{beta}} = 4.962 \times 10^{-10} \text{ yr}^{-1}$   
 $\lambda_{\text{epsilon}} + \lambda_{\text{epsilon}'} = 0.581 \times 10^{-10} \text{ yr}^{-1}$   
 $40\text{K}/\text{K} = 1.193 \times 10^{-4} \text{ g/g}$   
 $40\text{Ar}^* = \text{radiogenic Ar}$

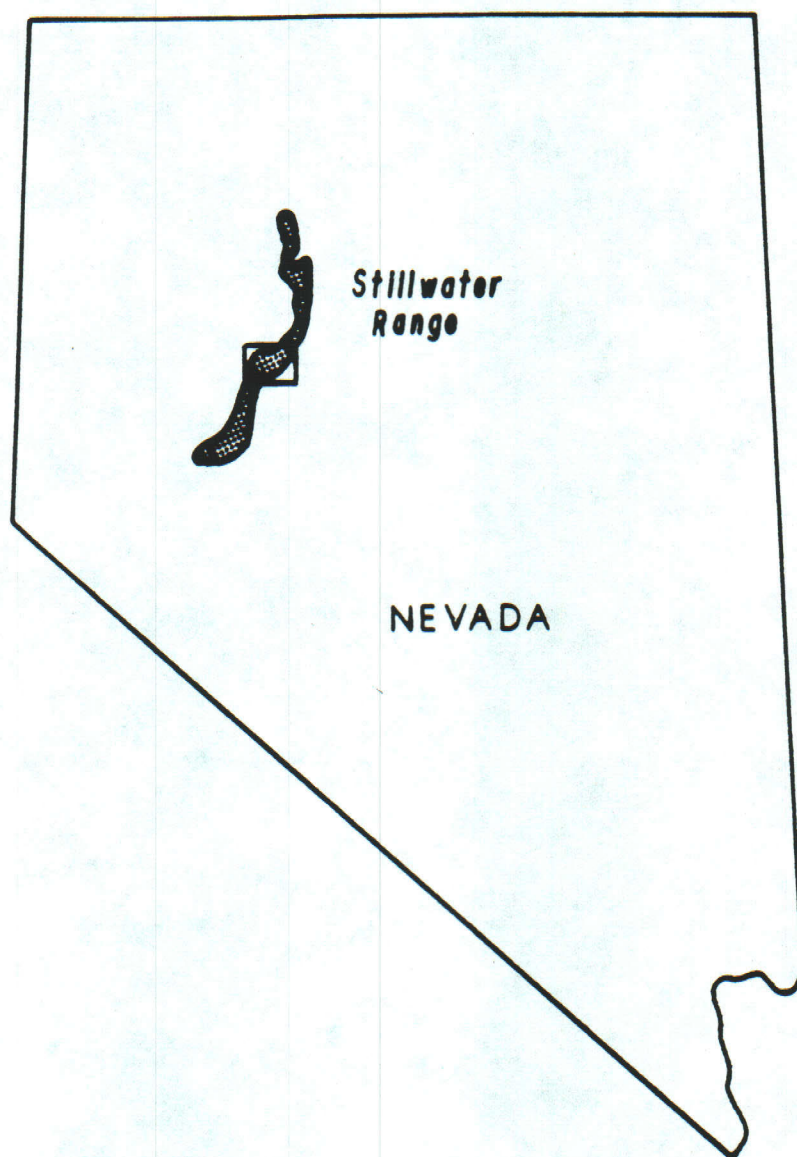
Table 2. Characteristics of major fluid inclusion groups.

Property	Type I Moderate Salinity	Type II CO <sub>2</sub> bearing	Type III Low Eutectic	Type IV halite
Phases at room T	40-90%l 10-60%v	60 to 90% H <sub>2</sub> O l 10 to 40% CO <sub>2</sub> l + CO <sub>2</sub> v	80-90%l 0-20%v	H <sub>2</sub> O l H <sub>2</sub> O v  10% NaCl
aqueous phase at low T	freeze at -30 to -40 melting of last solid (ice) 0 to -11		freeze at -60 -80 coarsens -40 visible melt -40 melting of last solid ice -26 to -9	
Bubble Behavior at low T	no change	CO <sub>2</sub> melts -57.5 to -54.4		
Gas hydrates	none	clathrate melts 6.4 to 9.7°C		
Heating Behavior	homogenization to l at 125 to 400	CO <sub>2</sub> l-v 22.5-29.3(v) homogenization CO <sub>2</sub> l-v 25.4-29.4(l) to liquid 129-283 homogenization to l at 197 to 358		TmNaCl 160-356 ThL-V 275-382
Number of measurements	256	45	19	7

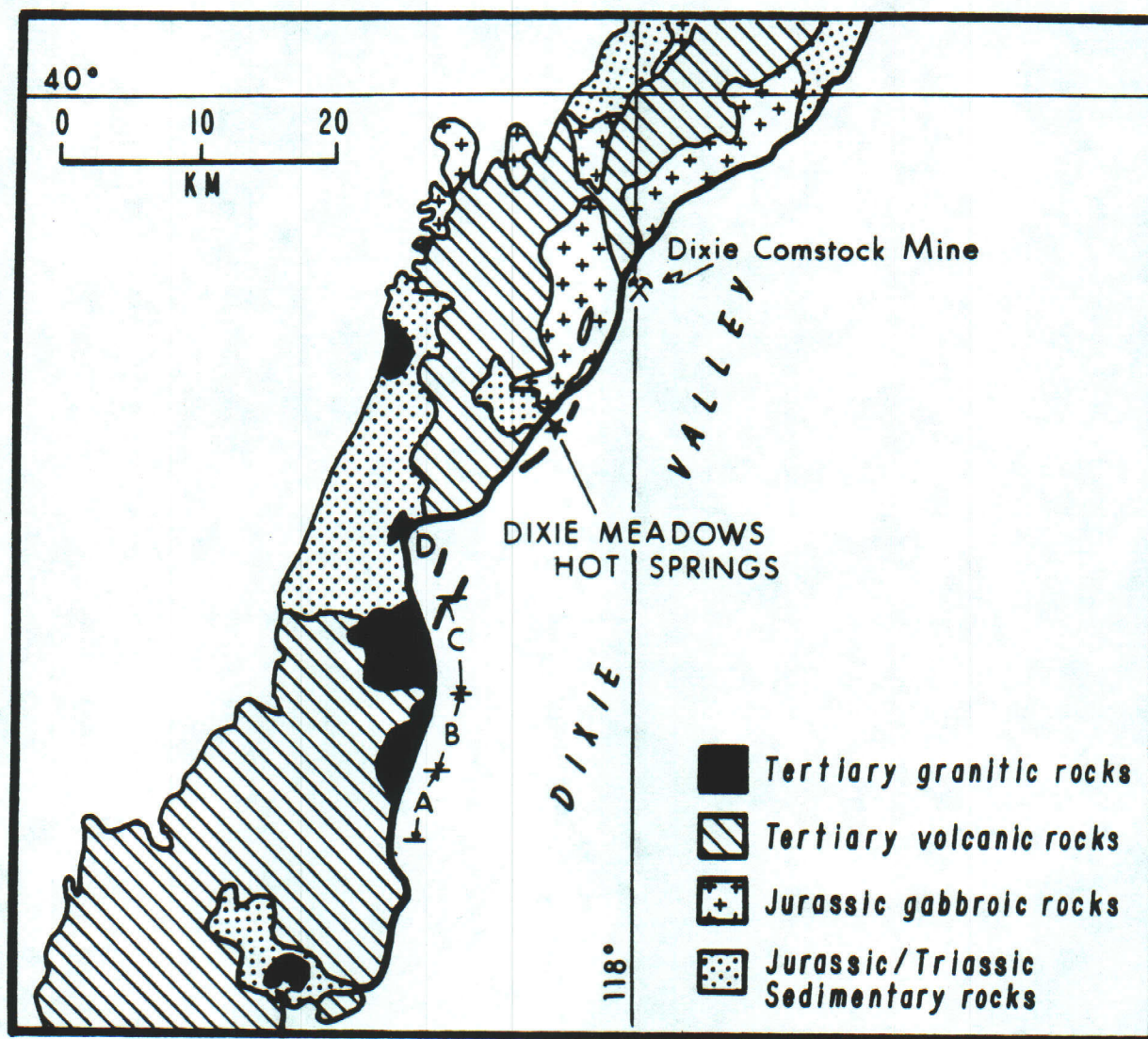
Table 3. Microthermometric properties of carbon dioxide bearing fluid inclusions.

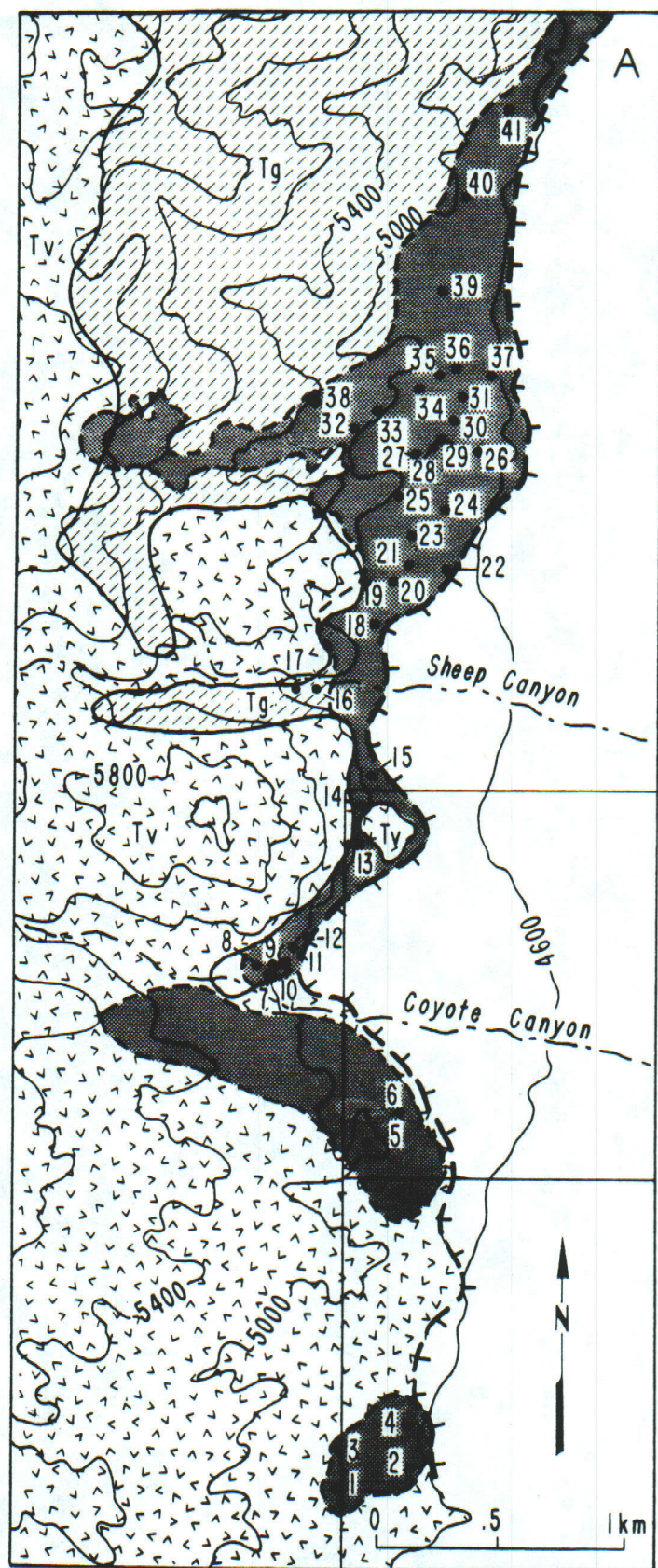
Map No.	Sample No.	TmCO <sub>2</sub>	TmCO <sub>2</sub> Clath	ThCO <sub>2</sub> L-V <sup>2</sup>	Th	Vol %CO <sub>2</sub>	WNaCl	XNaCl	XH <sub>2</sub> O	XCO <sub>2</sub>	P	
12	DV87-1f	1	-56.5	9.2	28.0v	304	30	1.63	0.005	0.931	0.065	390
		4	-56.9	8.4	20.5v	313	29	3.19	0.010	0.942	0.049	320
		8	-56.8	7.9	26.5v	297	27	4.14	0.012	0.933	0.055	360
		14	-57.4	9.7	27.9v	300	30	0.62	0.002	0.934	0.064	340
		15	-56.4	9.6	29.3v	278	25	0.82	0.002	0.939	0.058	340
		16	-57.6	7.9	28.0v	335	39	4.14	0.012	0.902	0.086	450
		17		9.0	27.1v	340	40	2.03	0.006	0.909	0.085	440
22	DV87-4	17	-56.8		29.4	270v						
		18	-56.7	9.7	22.5v	371v	80	0.62	0.001	0.726	0.272	
		19	-57.2	8.0	28.4l	239D	17	3.95	0.012	0.921	0.068	1100D
20	DV87-5a	8	-56.4			307						
		10	-56.5	8.4	16.8l	325		3.19				
		11	-57.0	8.5	26.6l	312D	42	3.10	0.008	0.810	0.182	1250D
		12	-57.5	8.5	26.2l	254D	25	3.10	0.008	0.890	0.102	1170D
		13		8.2	29.0l	197	9	3.67	0.011	0.947	0.042	540
18	DV87-7	5	-56.3	8.5	27.2v	312v		3.10	0.009	0.066	0.068	
		6	-56.3	8.5	26.4v	280	23	3.10	0.009	0.943	0.048	350
		7	-56.3	8.1	27.5v	308	31	3.86	0.011	0.924	0.065	380
		8	-56.3	8.6	22.5v	318	32	2.91	0.008	0.935	0.056	340
43	DV87-19	1	-56.4	7.1	24.7v	80v?	90	5.59	0.009	0.479	0.512	
		2	-56.9	6.9	24.0v	210D	15	6.03	0.018	0.948	0.033	320D
		6	-57.0	6.8	27.5v	250D	26	6.12	0.019	0.926	0.055	460D
		7	-57.1	7.9	28.0	261D	28	4.14	0.012	0.927	0.060	380D
69	DV87-33a	7	-57.2		13.5l	100						
87	DV87-52a	8		7.3		358						
D	DV87-54a	1	-55.4	8.5	26.5l	240D	21	3.00	0.009	0.906	0.085	1070D
		2	-55.1	9.1	27.2l	252D	25	1.83	0.005	0.895	0.100	1100D
		3	-54.9	8.1	25.4l	280	31	3.76	0.010	0.856	0.134	1480
		4	-54.4	8.0	27.0l	268	27	3.95	0.011	0.881	0.108	1300
		5	-56.7	7.6	28.7v	324	34	4.69	0.014	0.910	0.076	550
		6	-56.5	7.8	28.4v	320	36	4.32	0.013	0.907	0.080	430
		7	-56.8	7.8	27.5v	303	30	4.32	0.013	0.924	0.063	370
D	DV87-55	1	-56.7	8.3	30.0v	234	14	3.38	0.010	0.950	0.039	360
		3	-56.5	7.7	29.4l	208	10	4.51	0.014	0.939	0.047	670
		5		7.9	29.0v	244	21	4.14	0.012	0.908	0.082	880
D	DV87-59	1	-56.0	7.9	27.5v	219	10	4.14	0.013	0.958	0.030	280
		2	-56.0	9.2	29.5v	216	10	1.63	0.005	0.963	0.032	310
		3	-55.6	8.9	28.9v	222	11	2.22	0.007	0.961	0.033	300
		4	-56.6	8.4	29.4l	279	33	3.19	0.009	0.866	0.126	1060
		5	-56.6	8.4	29.5l	287	32	3.19	0.009	0.866	0.125	1200
		7	-56.7	6.4	24.1l	268D	25	6.81	0.020	0.875	0.105	1560D
		9	-55.2	6.7	17.3l	248	18	6.29	0.019	0.908	0.073	1250
		10	-56.8	7.4	27.6l	259	19	5.05	0.015	0.909	0.076	1380
		11	-56.8	6.9	28.3l	305	32	5.94	0.017	0.857	0.126	1570
		12	-55.6	8.2	26.2l	294	39	3.57	0.009	0.824	0.167	1450

v, homogenizes to vapor phase; l, homogenizes to liquid phase. Map number on Figure 2 and Figure 3.



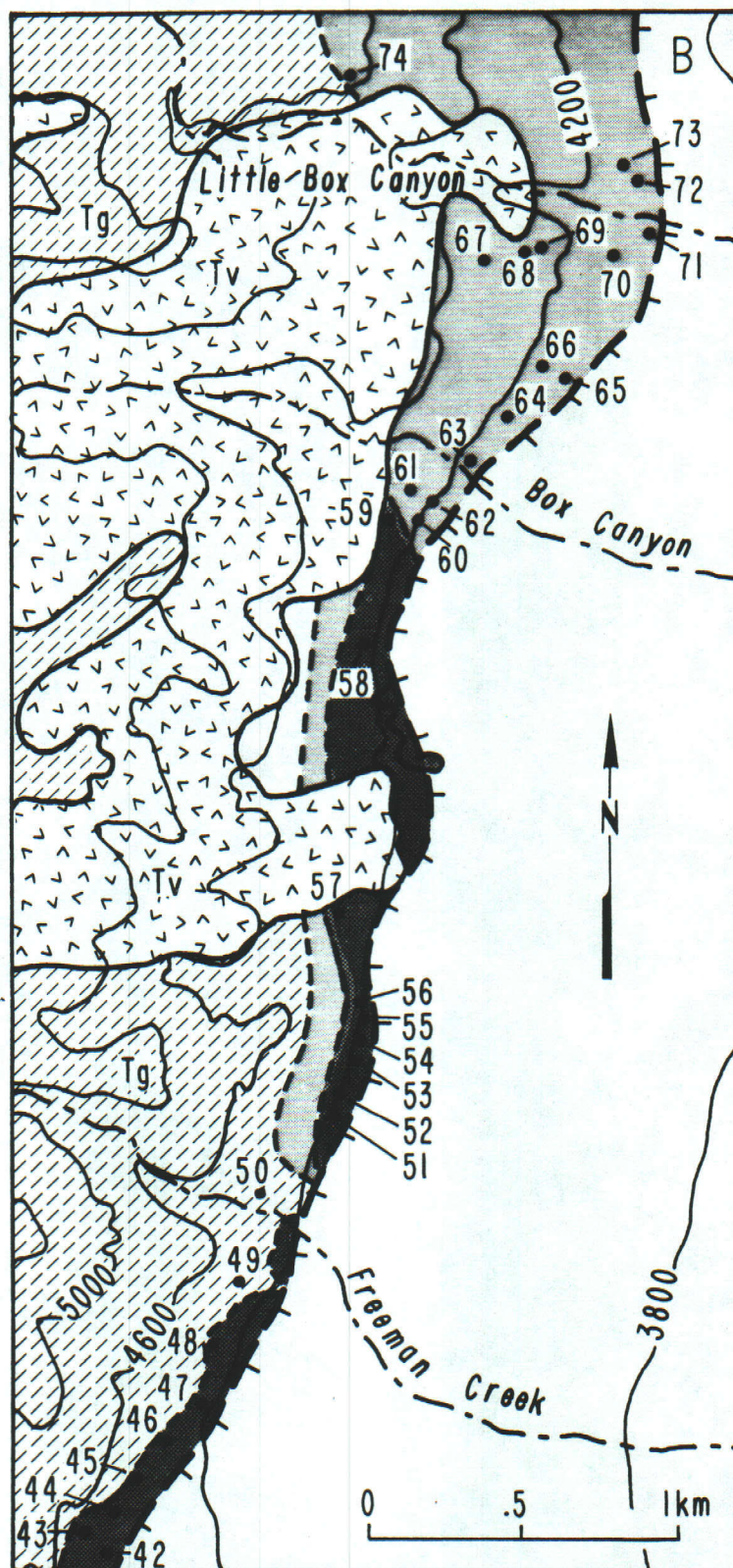
Parry et al. FIGURE 2

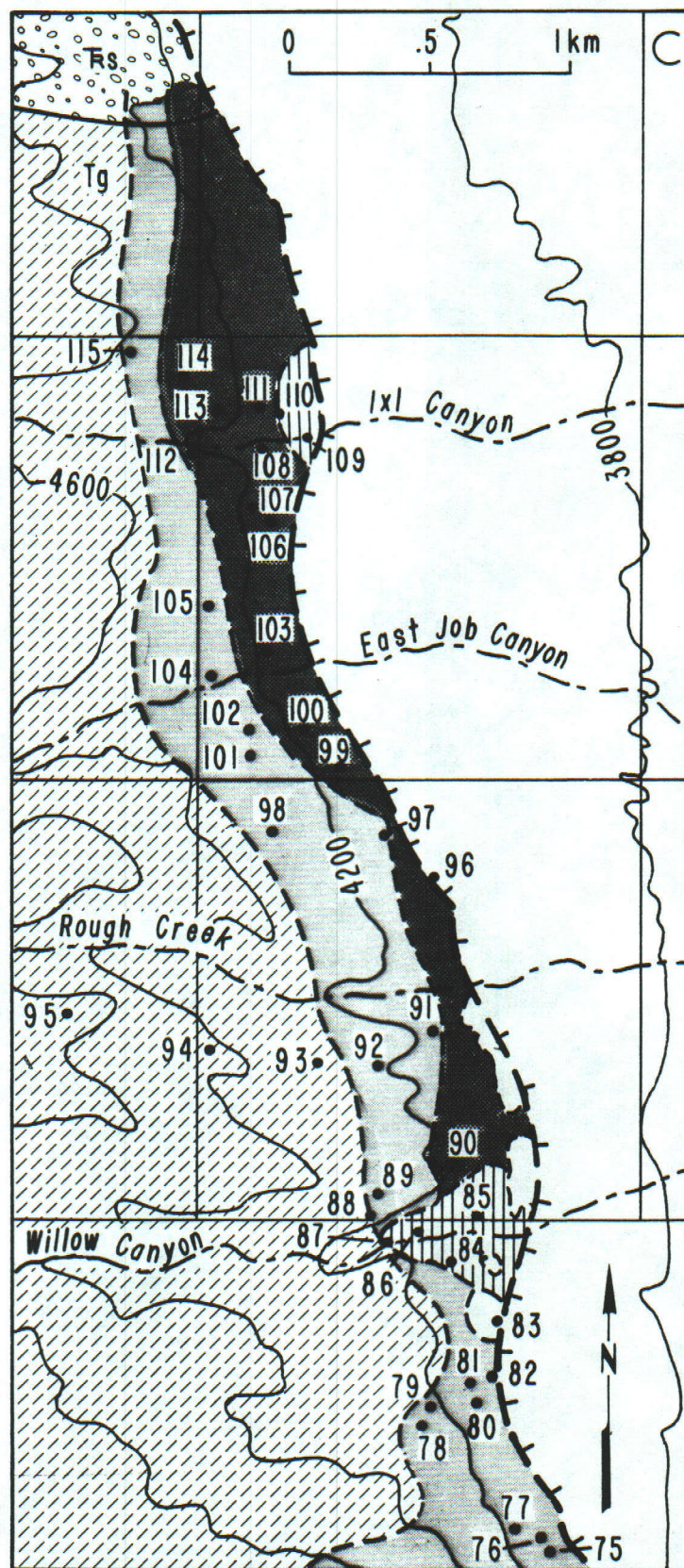


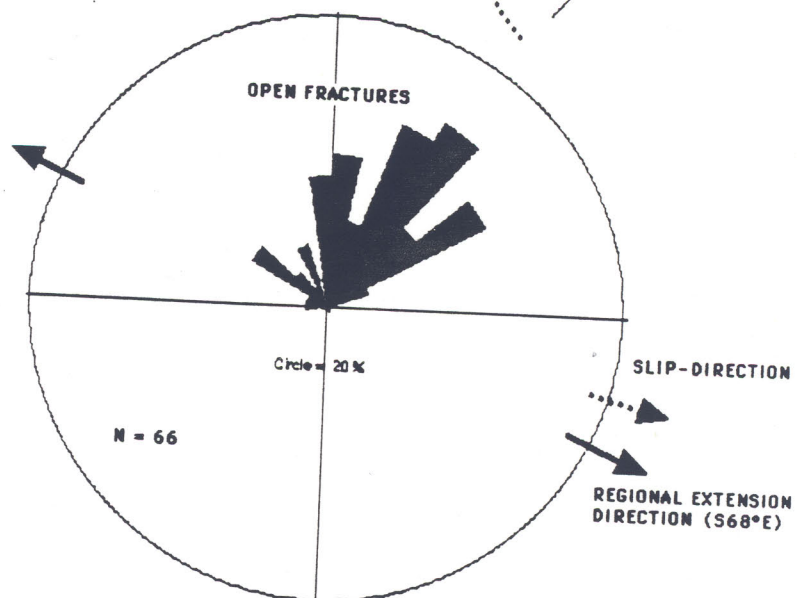
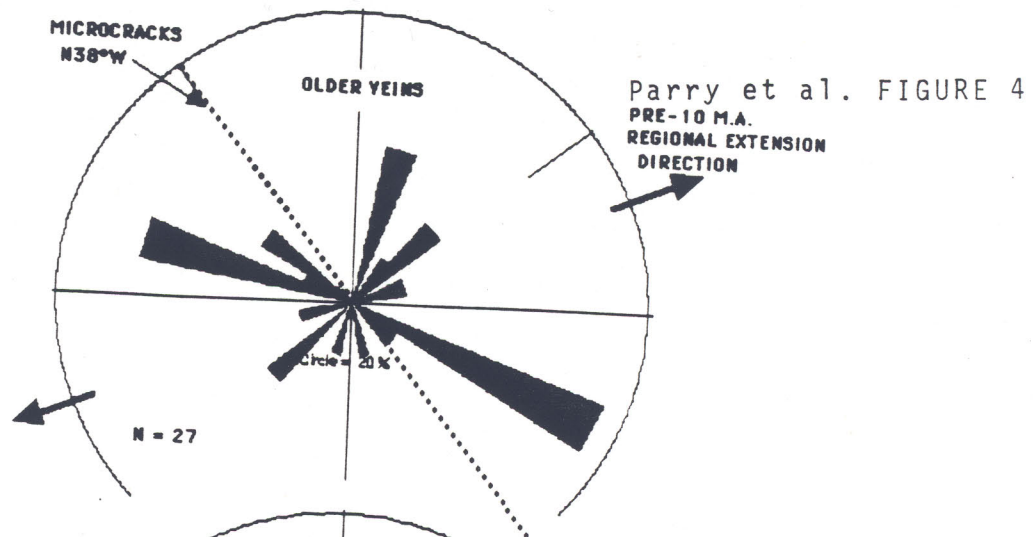


# EXPLANATION

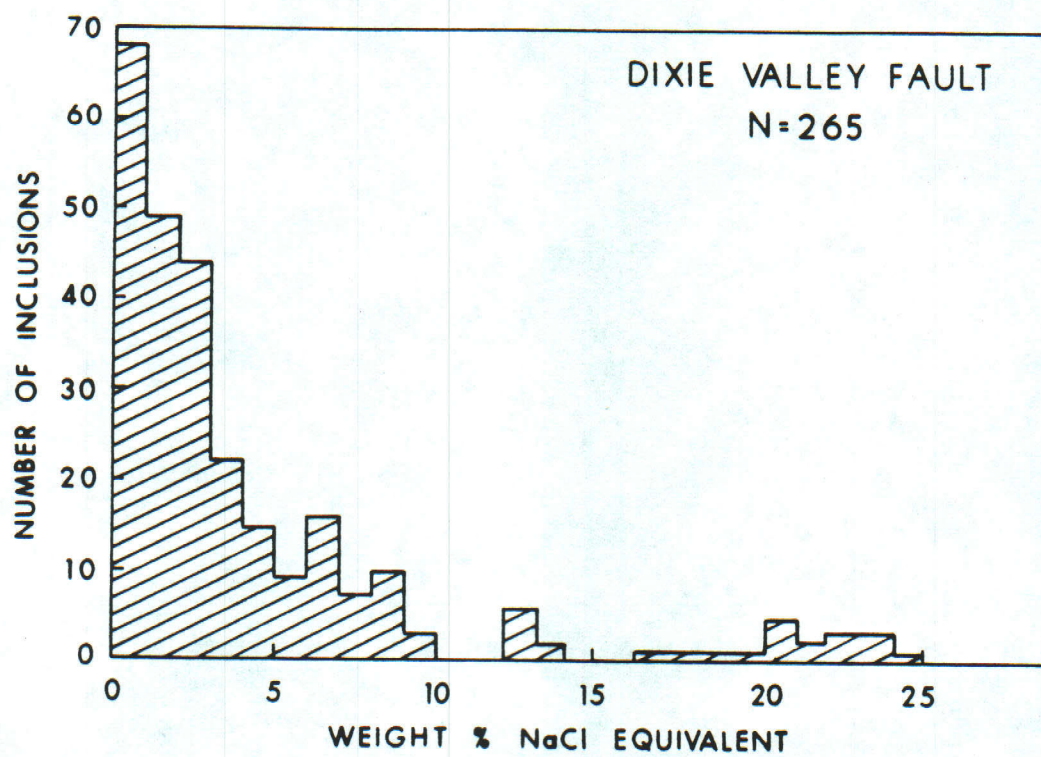
- Triassic sedimentary rocks
- Tertiary volcanic rocks
- Least altered granitic rocks
- Quaternary alluvium
- Chlorite and epidote alteration
- Sericite alteration
- Zeolite alteration
- Dixie Valley Fault
- 23 Sample locality

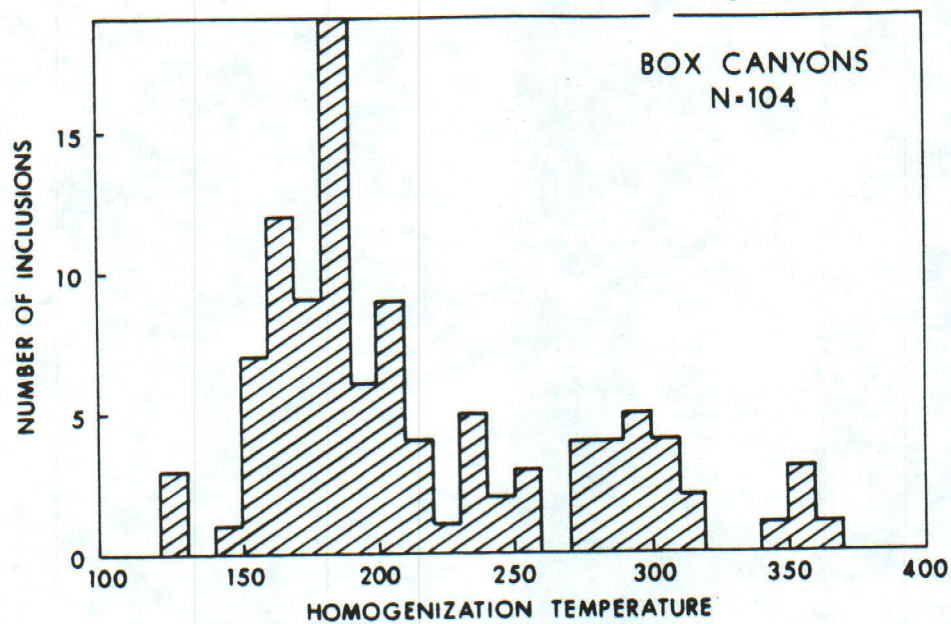




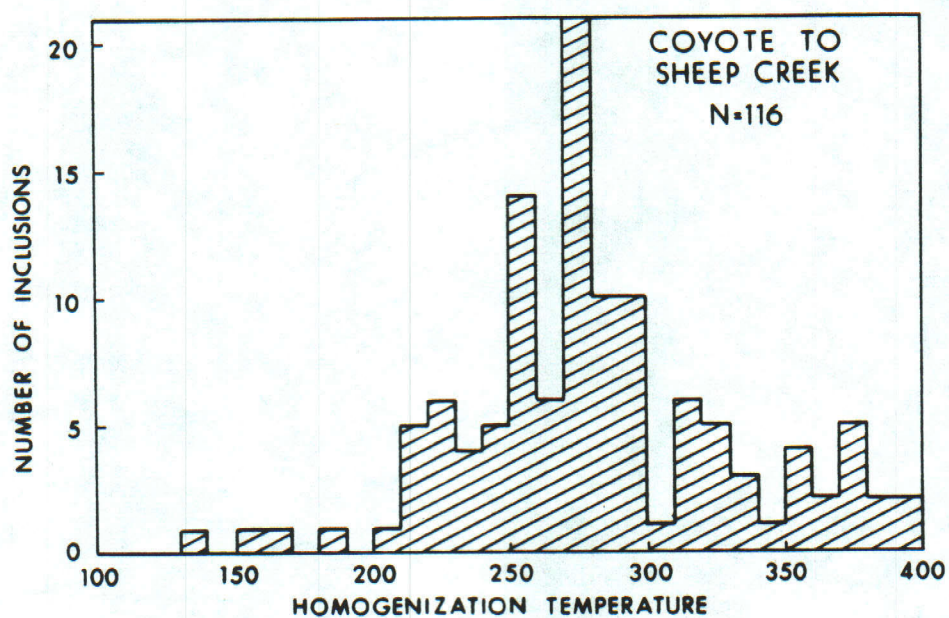


Parry et al. FIGURE 6

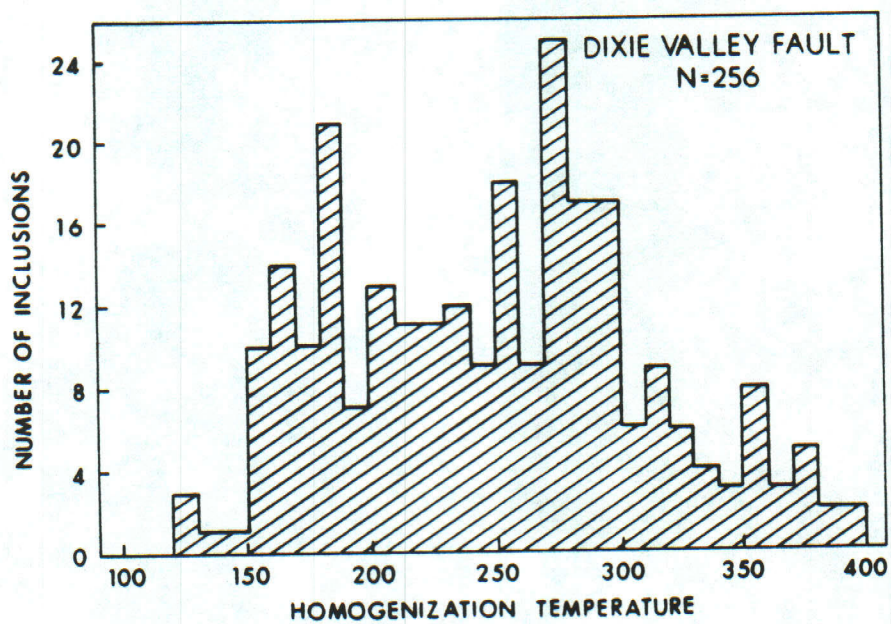




C

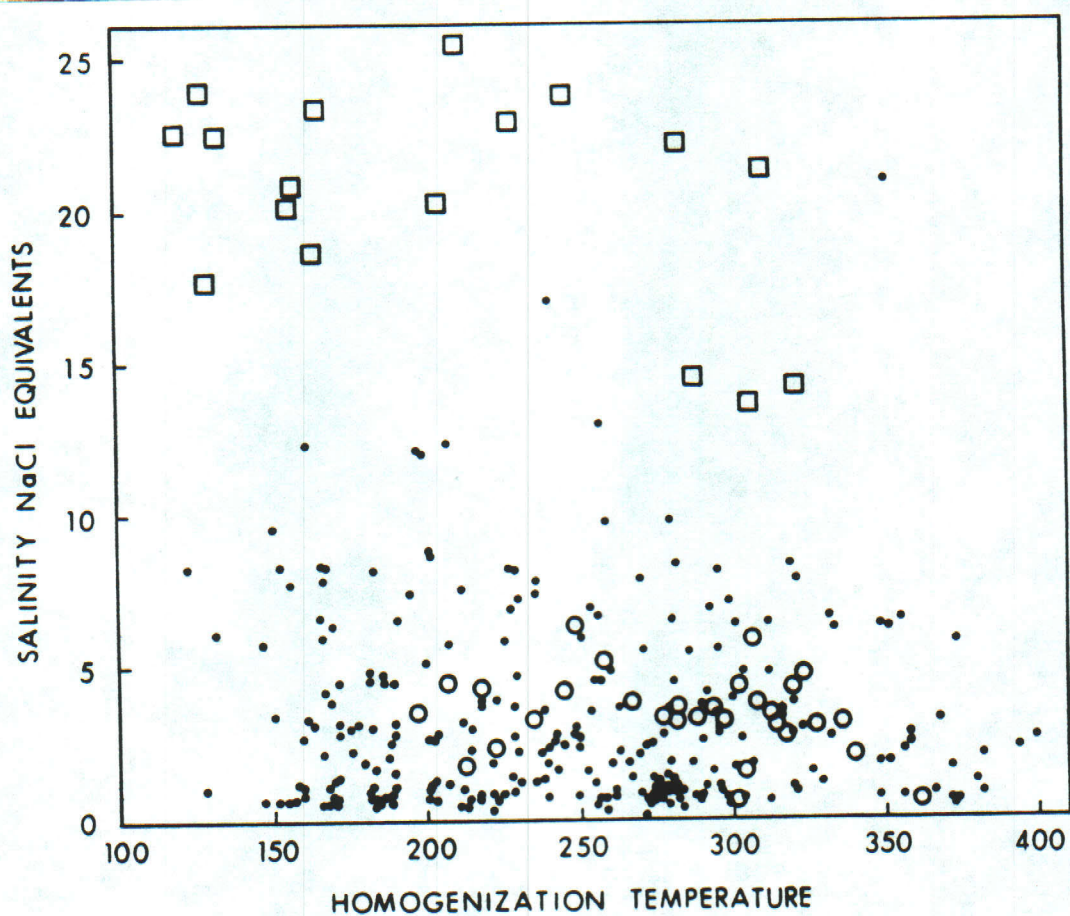
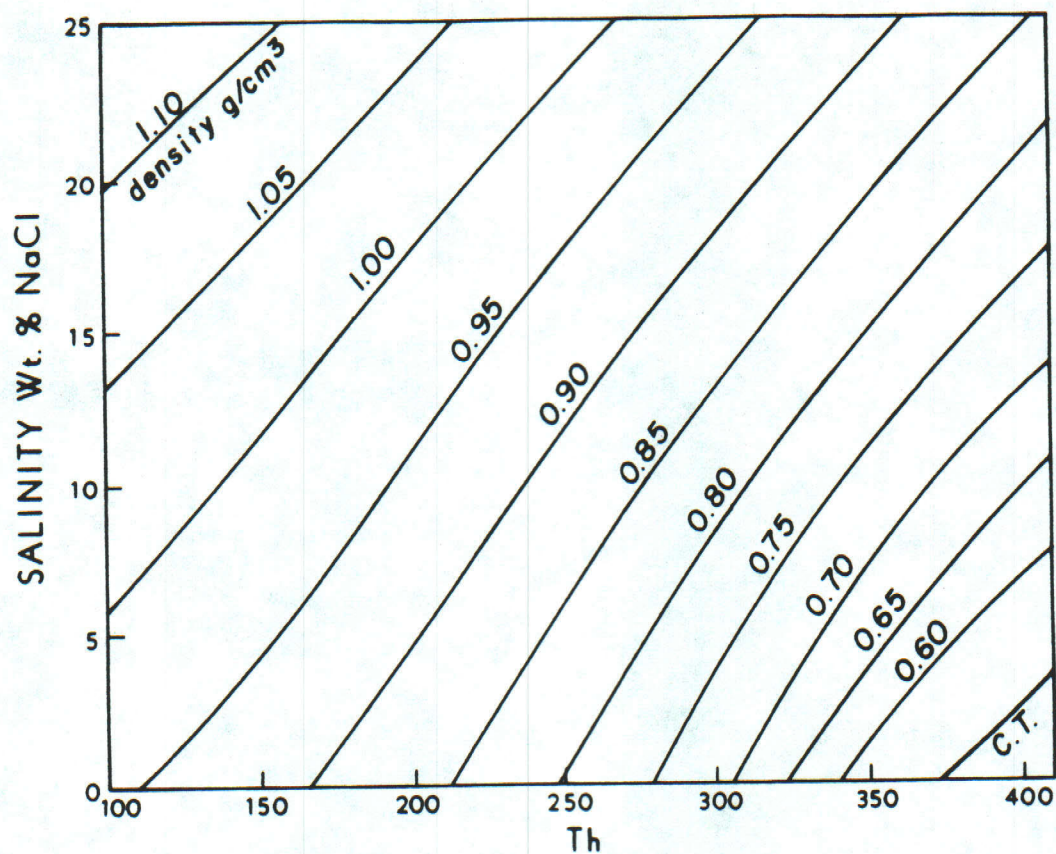


B

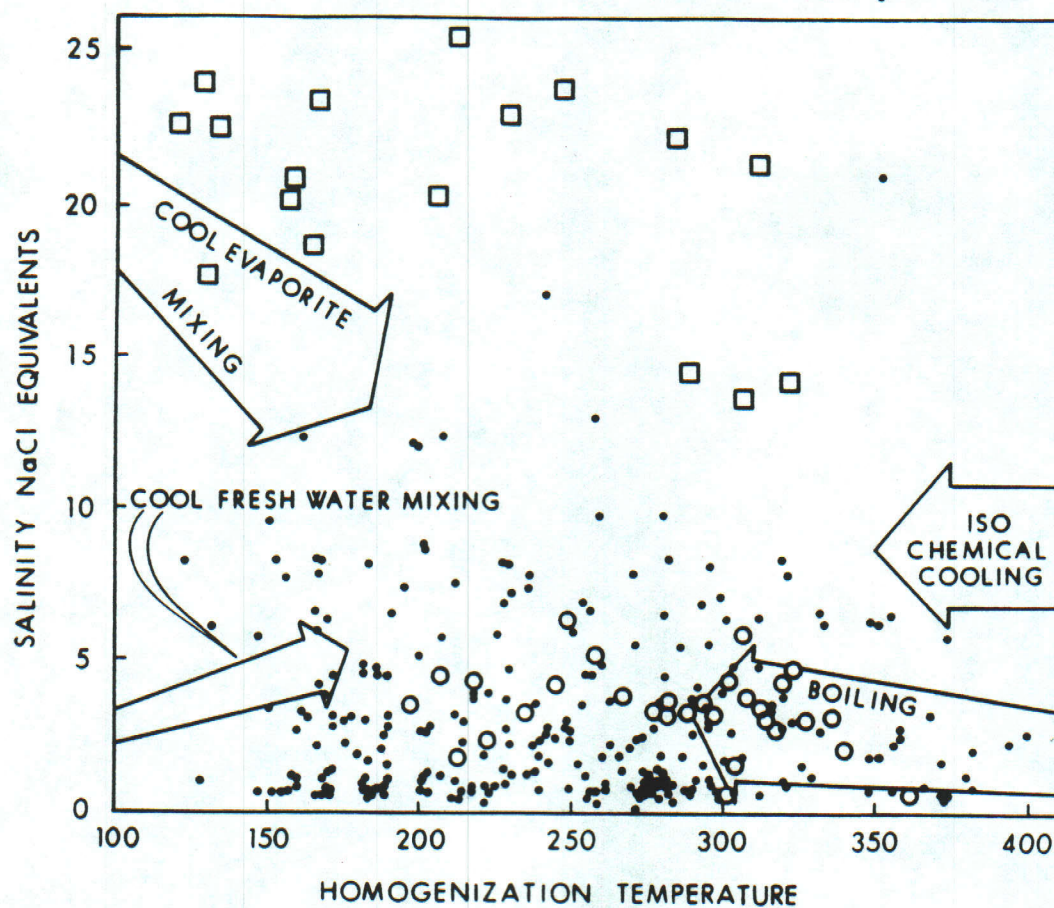


A

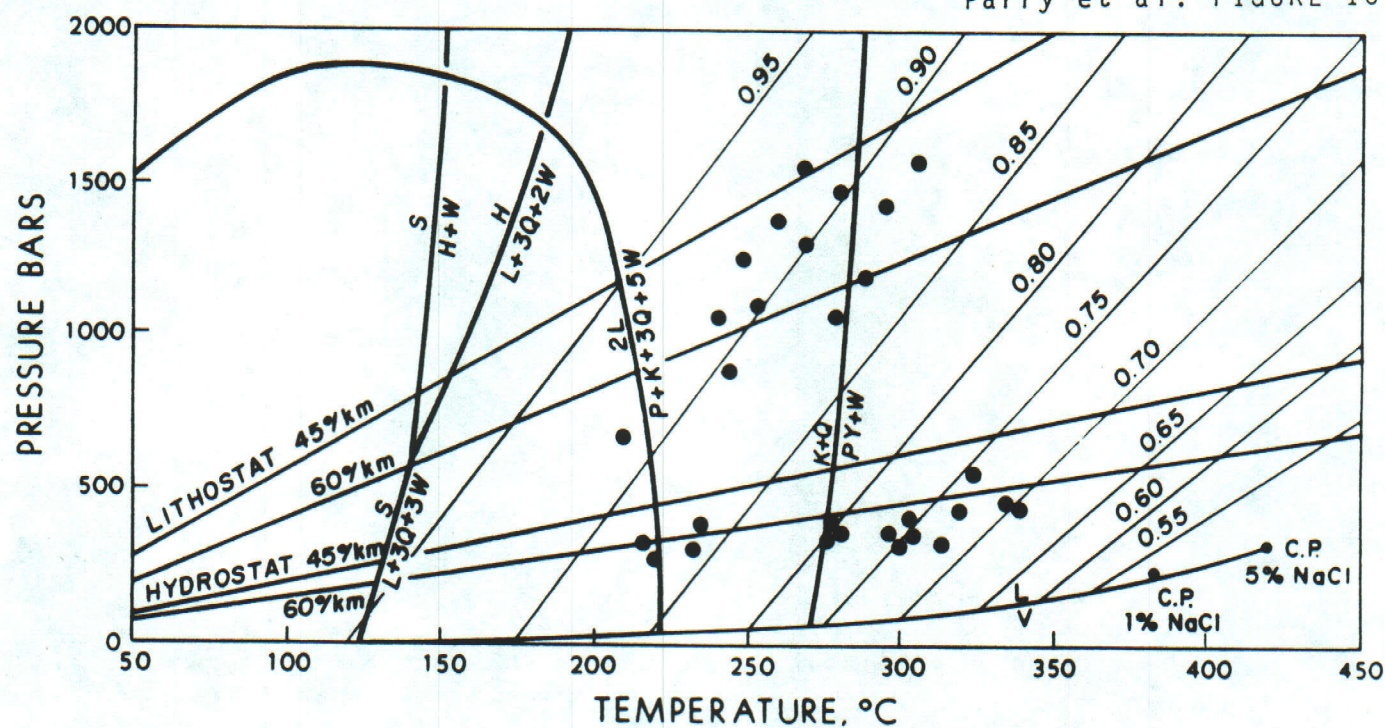
Parry et al. FIGURE 8

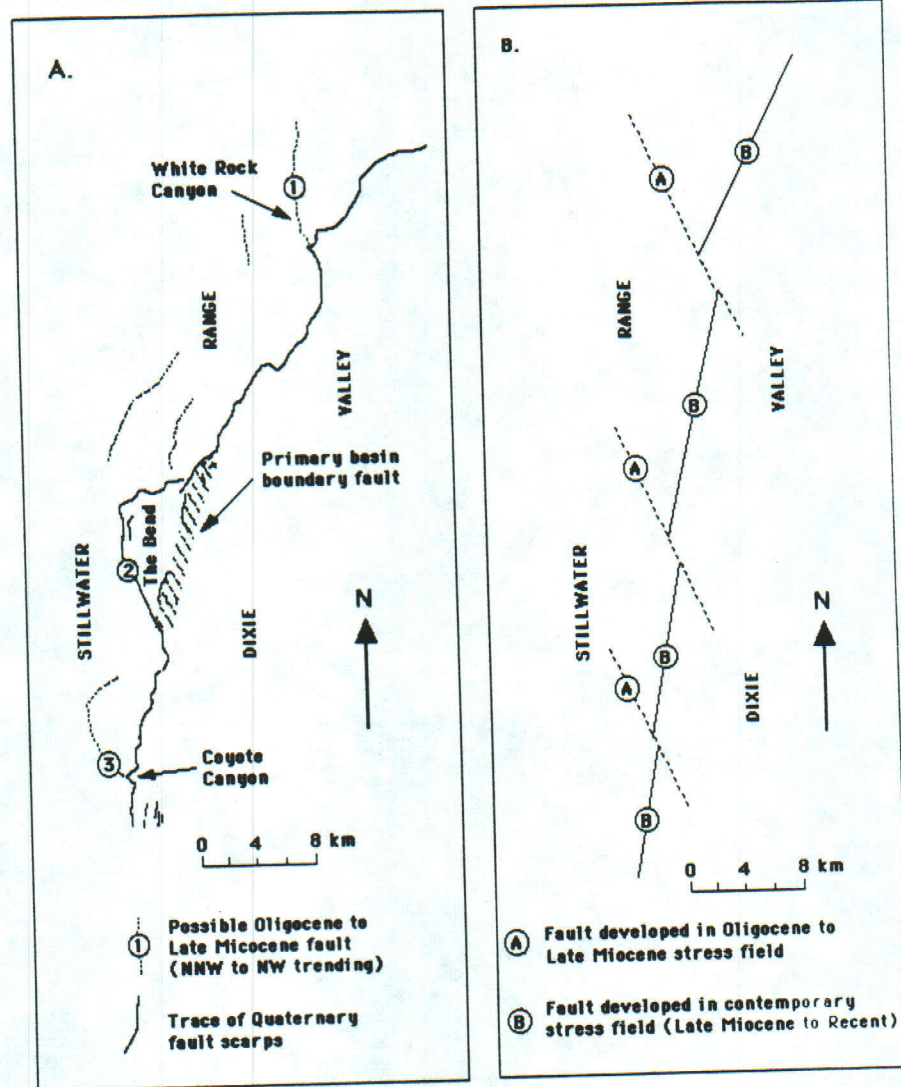


Parry et al. FIGURE 9



Parry et al. FIGURE 10







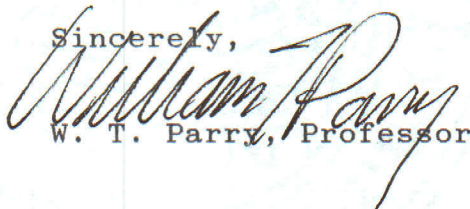
January 28, 1991

Jonathon G. Price, Director/State Geologist  
Nevada Bureau of Mines and Geology  
Mail Stop 178  
University of Nevada, Reno  
Reno, Nevada 89557-0088

Dear Mr. Price:

Enclosed is a DRAFT copy of our paper "Fluid Inclusions and Hydrothermal Alteration of the Dixie Valley Fault, Nevada". The manuscript includes our mapping of alteration along the footwall of the Dixie Valley fault, fluid inclusion analyses, and interpretations in terms of fault behavior. We are sending the manuscript to you partly in response to your request for maps of October 22, 1990, and partly because you and your colleagues may be interested in the results of our investigations.

Sincerely,



W. T. Parry, Professor

**Department of Geology and Geophysics**

College of Mines and Earth Sciences  
717 W. C. Browning Building  
Salt Lake City, Utah 84112-1183  
(801) 581-7162

FAX U of U Mines and Earth Sciences  
(801) 581-5560